CHALMERS
UNIVERSITY OF TECHNOLOGY

Automatic System Identification of Equivalent Circuit Parameters for Lithium Ion Batteries

Master's thesis in Mobility Engineering

RANJAN CHANDAR MANIMARAN

DEPARTMENT OF ELECTRICAL ENGINEERING
Division of Systems and Control

CHALMERS UNIVERSITY OF TECHNOLOGY
Gothenburg, Sweden 2025
www.chalmers.se

Master's thesis 2025

Automatic System Identification of Equivalent Circuit Parameters for Lithium Ion Batteries

A Master Thesis in Mobility Engineering

RANJAN CHANDAR MANIMARAN

CHALMERS
UNIVERSITY OF TECHNOLOGY

Department of Electrical Engineering
Division of Systems and Control
Chalmers University of Technology
Gothenburg, Sweden 2025

Automatic System Identification of Equivalent Circuit Parameters for Lithium Ion Batteries

RANJAN CHANDAR MANIMARAN

Supervisor: Anton Klintberg, Electromobility & Powertrain Systems(BMS Software & Controls), Polestar Performance AB
Examiner: Torsten Wik, Department of Systems & Controls, Electrical Engineering, Chalmers University of Technology

Master's Thesis 2025
Department of Electrical Engineering
Division of Systems and Control
Chalmers University of Technology
SE-412 96 Gothenburg
Telephone +46 31 772 1000

Cover: Calculating equivalent circuit model parameters that describe the voltage response of the cells to an applied current.

Typeset in LaTeX
Printed by Chalmers Reproservice
Gothenburg, Sweden 2025

Automatic System Identification of Equivalent Circuit Parameters for Lithium Ion Batteries

RANJAN CHANDAR MANIMARAN
Department of Electrical Engineering
Division of Systems and Control
Chalmers University of Technology

Abstract

Lithium-ion batteries are a critical component of electric vehicles (EVs), directly influencing their performance, range, and longevity. Battery management algorithms often rely on equivalent circuit models (ECMs) to describe the voltage response of cells to applied currents. However, accurately identifying ECM parameters is challenging due to their dependency on factors such as temperature, state of charge (SOC), and hysteresis. These challenges are further compounded by the time-consuming nature of the parameter identification process.

This thesis presents a novel system for identifying ECM parameters by executing realistic drive cycle current profiles on lithium-ion cells. The method accounts for temperature effects, SOC variations, and the hysteresis effect to improve modeling accuracy. The identified parameters were validated and stored in lookup tables for integration into battery management systems (BMS). The results demonstrated consistent parameter identification across various SOCs and temperatures, with a notable enhancement in ECM accuracy. Despite some limitations, such as challenges in parameter estimation at low temperatures, this work provides a robust foundation for more accurate and efficient BMS algorithms, particularly in automotive applications.

Keywords: Battery Management Algorithms, Equivalent Circuit Models, Battery Test Equipment

Acknowledgments

The thesis was carried out at Polestar Performance AB. First and foremost, I want to express my heartfelt gratitude to my company supervisor, Anton Klintberg, for providing me with the opportunity to engage in this remarkable thesis project. The successful completion of any endeavor in this project, at any level, relies significantly on the support and guidance provided by him.

I am also profoundly grateful to Jens Groot, whose assistance in the cell lab was indispensable. His expertise and support in addressing my doubts regarding modeling were crucial to the progress of my work. Special thanks go to my manager, Henrik Ohlsson, for his unwavering support and insightful advice, which were vital in navigating the practical aspects of the project.

Additionally, I extend my heartfelt thanks to all the colleagues and staff at Polestar Performance AB who contributed their time and knowledge to help me achieve my objectives. Your collaboration and support have been invaluable.

I would also like to thank my examiner and advisor, Torsten Wik, for his constructive feedback and continuous support. His insightful comments and guidance played a significant role in shaping this thesis into its final form.

Finally, I wish to acknowledge the love and support of my family and friends, whose encouragement and understanding provided the emotional foundation that enabled me to persevere through this journey.

Ranjan Chandar Manimaran, Gothenburg, June 2024

List of Acronyms

Below is the list of acronyms that have been used throughout this thesis listed in alphabetical order:

BMS	Battery Management System
CAN	Controller Area Network
CC	Constant Current
CV	Constant Voltage
DOC	Depth of Charge
DOD	Depth of Discharge
ECM	Equivalent Circuit Model
EVs	Electric Vehicles
GITT	Galvanostatic Intermittent Titration Technique
HPPT	Hybrid Pulse Power Characterisation
LFP	Lithium Ferro Phosphate
LSE	Least Square Error
NMC	Nickel Manganese Cobalt
OCV	Open Circuit Voltage
RMSE	Root Mean Square Error
SOC	State of Charge
SOH	State of Health
UDDS	Urban Dynamo-meter Drive Schedule

Nomenclature

Below is the nomenclature of indices, sets, parameters, and variables that have been used throughout this thesis.

$C1, C2$	Capacitance
$\dot{z}$	Rate of change of SOC
η	Coloumbic efficiency
i	Current
$M(z, \dot{z})$	Maximum hysteresis
M_0	Instantaneous hysteresis
N	Number of data points
Q	Capacity of the battery
R_0, R_1, R_2	Resistances
$RCpair$	Resistance Capacitance Pair
$\triangle t$	Sampling interval
v	Voltage
v_h	Hysteresis Voltage
v_{oc}	Open circuit voltage
γ	Rate of decay
k	Index of time step
z	State of Charge

Contents

List of Figures

1
Introduction

In recent years, electric vehicles (EVs) have emerged as a key solution for achieving global sustainability goals and reducing greenhouse gas emissions. Lithium-ion batteries, the core component of EVs, play a critical role in determining their range, performance, and overall capability. Effective management of these batteries is essential for optimizing their performance and lifespan, and this is typically achieved through advanced battery management systems (BMS).

A fundamental aspect of BMS is the equivalent circuit model (ECM), which simulates the battery's voltage response to various current profiles. The accuracy of the ECM is paramount for reliable state of charge (SoC), state of health (SoH), state of power estimation, and other critical functions. However, identifying ECM parameters is challenging due to their dependency on temperature, SoC, C-rates, and aging effects. Furthermore, the hysteresis effect, where the voltage response depends on previous states, complicates parameter identification. These challenges necessitate methods that account for such complexities while using realistic drive cycle current profiles.

This thesis develops a novel method to identify ECM parameters by executing realistic drive cycle current profiles, accounting for temperature effects and hysteresis, and storing the results in lookup tables for algorithm integration. The identified parameters provided consistent results across a range of SOCs and temperatures, with a significant improvement in modeling accuracy. The hysteresis effect was also successfully incorporated into the ECM for more realistic voltage predictions. This work enables more robust and accurate BMS algorithms, particularly in automotive applications.

1.1 Goal

The aim of the project was to develop a script that effectively controls battery test equipment. The script executed a predefined drive cycle current profile on lithium-ion cells while simultaneously tracking the state of charge (SOC) of the battery and the temperature within the thermal chamber. Subsequently, the voltage responses to the input current were recorded and imported into a separate script designed to identify the parameter values for the specified operating range. Additionally, a lookup table was created to store distinct sets of parameter values for both charging and discharging processes across the SOC range and for various temperatures.

These parameter sets can be utilized in battery management algorithms for more accurate battery performance modeling and management. The objectives of this project included:

1. To develop methods for accurately identifying ECM parameters

2. To investigate the impact of different current profiles on identification accuracy.

3. To analyze how parameters varied over a range of SOC and temperatures.

4. To model the hysteresis effect of the battery to enhance the accuracy of the ECM.

1.2 Limitations

While this project aimed to significantly enhance the process of ECM parameter identification, several limitations must be acknowledged:

1. **Complexity of Battery Behavior**: Lithium-ion batteries demonstrate highly intricate behavior that might not be fully encapsulated by equivalent circuit models, especially under extreme operating conditions.

2. **Test Equipment Constraints**: The precision and capabilities of the battery test equipment utilized significantly influenced the accuracy of parameter identification. It was constrained by its maximum recording speed between data-points of 10 milliseconds. As a result, reactions occurring faster than this interval may not have been captured.

3. **State of Health (SOH) Considerations**: This study did not explore how state of health (SOH) affects the parameters of the battery due to its potential to significantly expand the scope of the thesis and require substantial additional time and resources.

4. **Bias Towards Automotive Applications**: The utilization of drive cycle current profiles biased the model towards automotive applications. Other applications might require different testing methodologies.

5. **Temperature Range**: The investigation was limited to a temperature range of 0 to 40 degrees Celsius, potentially excluding behavior outside this range.

6. **Cell Chemistry Variation**: The focus of this work was on Lithium Iron Phosphate (LFP) cells. The equivalent circuit model parameters and hysteresis model may differ for cells of different chemistries.

7. **Coulombic Efficiency Assumption**: The Coulombic efficiency for charging and discharging was assumed to be 100% ($\eta = 1$). In reality, Coulombic efficiency can vary due to factors such as aging, temperature, and operating conditions, which may affect the accuracy of the parameter identification.

2

Theory

The following sections provide a comprehensive explanation of all the relevant theory necessary for conducting this thesis project and for appropriately interpreting the results.

2.1 Cells

Cells are the smallest individual electrochemical unit that delivers a voltage depending upon its chemistry. There are two types of cells :

1. Primary Cells
2. Secondary Cells

2.1.1 Secondary cells

Secondary cells are designed to be recharged and used multiple times. The electrochemical reactions in these batteries are reversible, allowing the chemical compounds to be restored to their original state by applying an electrical potential between the electrodes. This reversibility enables the battery to be recharged and reused multiple times, providing a cost-effective and environmentally friendly solution for powering devices.
Example :

- Lithium-ion Batteries: Widely used in smartphones, laptops, electric vehicles, and power tools. (e.g., 18650 cells, smartphone batteries)

2.2 Function Components of Electrochemical Cell

2.2.1 Negative Electrode

The negative electrode, also known as the anode during discharge, is typically composed of a metal or an alloy. Its primary function is to release electrons to the external circuit during the discharge process, undergoing oxidation. Conversely, during charging, it accepts electrons from the external circuit and undergoes reduction. Common materials for the negative electrode include graphite in lithium-ion batteries and zinc in alkaline batteries.

2.2.2 Positive Electrode

The positive electrode, or cathode during discharge, is usually made from a metallic oxide, sulphide, or oxygen-containing compounds such as lead dioxide in lead-acid batteries. During discharge, it gains electrons from the external circuit and undergoes reduction. During charging, the process reverses; it loses electrons to the external circuit and undergoes oxidation. Examples of materials used for the positive electrode include lithium cobalt oxide in lithium-ion batteries and manganese dioxide in alkaline batteries.

2.2.3 Electrolyte

The electrolyte is a critical component that facilitates ion movement within the cell while maintaining electronic insulation to prevent short circuits. As electrons traverse the external circuit, the electrolyte allows for compensating ion migration internally:

- **Cations** are positively charged ions that move towards the positive electrode (cathode) during discharge.
- **Anions** are negatively charged ions that move towards the negative electrode (anode) during discharge.

The electrolyte typically comprises a solvent containing dissolved salts, acids, or bases that provide ionic conductivity. For instance, in a lithium-ion battery, the electrolyte may be a lithium salt dissolved in an organic solvent.

2.2.4 Separator

The separator is a vital component that electrically insulates the positive and negative electrodes, preventing short circuits and self-discharge of the cell. It is usually made from porous materials such as glass mat, fiber, or polymers. The separator allows ion flow while blocking the direct passage of electrons, ensuring the safe operation of the cell.

2.2.5 Current Collectors

Current collectors are essential for conducting electrical current from the electrodes to the external terminals of the cell. The electrodes themselves are often composed of active material powders that are adhered to metal foil current collectors. These collectors, typically made from metals such as copper for the anode and aluminum for the cathode in lithium-ion batteries, provide a conductive path for electrons to flow to and from the cell terminals, ensuring efficient energy transfer.

2.3 Working of Lithium Ion Batteries

Lithium-ion cells are composed of four fundamental components: the positive electrode, the negative electrode, a separator, and an electrolyte (See Figure 2.1). Typically, the negative electrode is made of graphite, while the positive electrode can be

composed of various materials. The separator functions as an electrically insulating membrane that permits the passage of lithium ions [6].

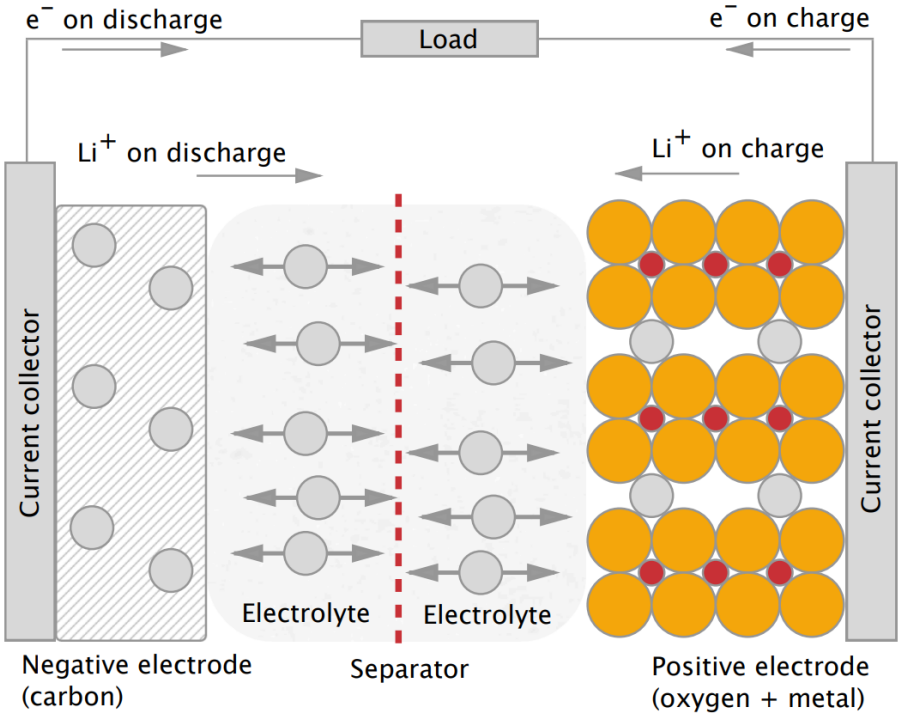

Figure 2.1: Schematic view of a lithium ion cell [6]

During discharge, lithium ions migrate from the negative electrode to the positive electrode through a process known as intercalation. Concurrently, electrons travel through an external circuit, generating electrical energy. This process is reversed during charging.

The cell's energy is determined by the difference in energy states of lithium ions intercalated within the positive and negative electrodes. When the cell is at equilibrium, these potentials are called open circuit potentials (OCP) and gives rise to a potential difference referred to as the open circuit voltage (OCV). During operation, the cell voltage is influenced by concentration gradients within the cell. These gradients arise primarily due to solid-state diffusion, charge transfer resistance, and mass transport within the electrolyte.

2.4 Battery Construction and Configuration

Batteries are composed of multiple electrochemical cells connected together to achieve the desired voltage and capacity. These cells can be connected in series, in parallel, or a combination of both, depending on the specific requirements of the application.

2.4.1 Series Connection

When cells are connected in series, the total voltage of the battery is the sum of the individual cell voltages, while the capacity (in ampere-hours, Ah) remains the same as that of a single cell. This configuration is used to achieve higher voltages.
Example:

- In an electric vehicle, a 400V battery pack could be constructed by connecting 96 cells, each with a voltage of 4.2V, in series. This results in a total voltage of $96 \times 4.2V = 403.2V$.

2.4.2 Parallel Connection

In a parallel connection, the total capacity of the battery is the sum of the individual cell capacities, while the voltage remains the same as that of a single cell. This configuration is used to increase the overall capacity and current capability of the battery.
Example:

- If each cell has a capacity of 2Ah, connecting 5 cells in parallel would result in a battery with a total capacity of $5 \times 2Ah = 10Ah$.

2.4.3 Combination of Series and Parallel

For applications requiring both higher voltage and higher capacity, cells can be connected in a combination of series and parallel. This approach allows for flexible design and optimization of battery packs to meet specific energy and power requirements.

2.5 Cell Terminologies

2.5.1 Nominal Voltage

The nominal voltage of a cell is a characteristic value that depends on the specific combination of active chemicals used within the cell. It represents an average or typical voltage that the cell maintains under normal operating conditions, rather than the actual voltage under load, which can vary. For instance, nickel-based cells typically have a nominal voltage of 1.2V, while lithium-based cells usually have a nominal voltage of around 3V.

2.5.2 Nominal Capacity

The nominal capacity, also known as the total charge capacity, specifies the total amount of electric charge a cell can store, expressed in ampere-hours (Ah) or milliampere-hours (mAh). This capacity indicates the amount of charge the cell is rated to hold, which determines how long the cell can provide power at a specified current.

2.5.3 C Rate

The C rate is a measure of the rate at which a cell is charged or discharged relative to its maximum capacity. It is defined as the constant current rate that a cell can sustain over one hour. For example:

- A 20 Ah cell can deliver 20A (1C rate) for 1 hour or 2A (C/10 rate) for 10 hours.

This metric helps in understanding the cell's performance and how quickly it can be charged or discharged safely.

2.5.4 Energy and power

A cell stores energy in an electrochemical form, which can be later converted to perform work. The total energy storage capacity of a cell is approximately the product of its nominal voltage and nominal capacity.
Example:

- A cell with a nominal voltage of 3.7V and a nominal capacity of 1.9Ah has an energy storage capacity of $3.7V \times 1.9Ah = 7.03Wh$.

The rate at which this stored energy is released is termed as the cell's instantaneous power, measured in watts (W). Power is an important parameter as it determines how quickly the energy can be delivered to a load.

2.5.5 State of Charge

SOC refers to the remaining capacity of a battery relative to its full capacity, expressed as a percentage. It indicates how much energy is left in the battery compared to its maximum capacity.

2.5.6 Depth of Discharge

DOD is the percentage of a battery's capacity that has been discharged relative to its total capacity. It measures how much of the battery's energy has been used during a discharge cycle.

2.5.7 Cycle Life

Cycle life refers to the number of charge-discharge cycles a battery can undergo before its capacity significantly degrades. It is an important factor in determining the longevity and reliability of a battery system.

2.5.8 Coulombic Efficiency

Coulombic efficiency, also known as charge efficiency, is a key parameter that measures the efficiency of charge transfer within a battery. It is defined as the ratio of the actual charge delivered during discharge to the theoretical charge input during

charging. Mathematically, Coulombic efficiency η_c can be expressed as:

$$\eta_c = \frac{Q_{\text{discharge}}}{Q_{\text{charge}}} \times 100\%$$

2.6 Battery Management System

The Battery Management System (BMS) plays a critical role in ensuring the safe, reliable, and efficient operation of the battery pack. It acts as the brain of the battery system, overseeing and managing various functions to optimize performance and protect the battery from damage.

2.6.1 General BMS Functionality

2.6.1.1 Sensing and High Voltage Control

The BMS is equipped with sensors to monitor key parameters of the battery pack, including voltage, current, and temperature. High voltage control functions include:

- **Voltage Measurement:** Continuously monitors the voltage of individual cells and the overall pack to ensure they remain within safe operating limits.
- **Current Measurement:** Tracks the current flowing in and out of the battery pack to manage charge and discharge rates.
- **Temperature Measurement:** Uses temperature sensors to monitor the thermal conditions of the battery pack, crucial for preventing overheating and ensuring optimal performance.
- **Contactor and Relay Control:** Manages contactors and pre-charge relays to safely connect and disconnect the battery pack from the load or charger.
- **Ground Fault Detection:** Identifies insulation faults that could lead to dangerous conditions, ensuring electrical safety.
- **Thermal Management:** Actively manages heating and cooling systems to maintain the battery within its optimal temperature range.

2.6.1.2 Protection Against

The BMS protects the battery pack against various potentially damaging conditions, including:

- **Overcharge Protection:** Prevents cells from exceeding their maximum voltage, which can lead to overheating or damage.
- **Overdischarge Protection:** Ensures cells do not fall below their minimum voltage, which can cause capacity loss and reduce lifespan.
- **Overcurrent Protection:** Detects excessive current flow that could damage the battery or connected devices.
- **Short Circuit Protection:** Quickly disconnects the battery in case of a short circuit to prevent fires or explosions.
- **Extreme Temperature Protection:** Shuts down or limits battery operation in extreme temperatures to avoid thermal runaway or degradation.

2.6.1.3 Interface

The BMS interfaces with other systems and provides critical information, including:

- **Range Estimation:** Calculates the remaining range of the battery based on current SOC and usage patterns.
- **Communications:** Interfaces with external systems via protocols like CAN bus to exchange data with vehicle control units, chargers, and user interfaces.
- **Data Recording and Reporting:** Logs operational data for performance analysis, diagnostics, and regulatory compliance.

2.6.1.4 Performance Management

The BMS ensures optimal performance of the battery pack through:

- **State of Charge (SOC) Estimation:** Accurately estimates the SOC to provide reliable information on remaining capacity.
- **Power Limit Computation:** Determines safe power limits for charging and discharging to protect the battery and extend its life.
- **Cell Balancing:** Ensures all cells in the battery pack are at the same voltage level, preventing imbalances that can reduce capacity and lifespan.

2.6.1.5 Diagnostics

The BMS conducts continuous diagnostics to detect and address issues:

- **Abuse Detection:** Identifies abnormal conditions such as over voltage, over current, or excessive temperature that could indicate misuse or faults.
- **State of Health (SOH) Estimation:** Evaluates the battery's condition and remaining useful life, aiding in maintenance and replacement decisions.

3

Lithium Ion Cell Modelling Theory

3.1 Importance of Battery Modeling

Battery modeling plays a crucial role in the development and operation of Battery Management Systems (BMS). Accurate models enable the BMS to monitor and control the battery effectively, ensuring optimal performance, longevity, and safety. Battery management algorithms are often based on equivalent circuit models that describe the voltage response of the cells to an applied current. These models provide a simplified but accurate representation of the complex electrochemical processes within the battery.

3.1.1 Key Aspects of Battery Modeling

- **State Estimation:** Battery models are essential for estimating the State of Charge (SOC) and State of Health (SOH) of the battery. These states are not directly measurable and require accurate models to infer from measurable quantities such as voltage, current, and temperature. Precise state estimation is vital for predicting the remaining capacity and ensuring safe operation.
- **Predictive Control**: By understanding the battery's behavior under various conditions, the BMS can predict future states and take preventive actions to avoid damaging conditions. This includes avoiding overcharging, deep discharging, and operating outside safe temperature ranges.
- **Efficiency Optimization**: Accurate battery models help optimize the charging and discharging processes. The BMS can use these models to implement algorithms that maximize efficiency, reduce energy losses, and extend the battery's cycle life.
- **Thermal Management**: Battery models that include thermal characteristics enable the BMS to manage the temperature of the battery pack effectively. By predicting temperature changes, the BMS can activate cooling or heating systems to maintain the battery within an optimal temperature range, thereby enhancing performance and safety.

3.2 Lithium Ion Battery Models

There are several approaches to battery modeling, each with its own advantages and complexities. The main types of battery models are:

- Physics based modeling
- Empirical modeling
- Data driven modeling

3.2.1 Physics Based Modeling

Physical models start from the reactions inside the cell. Electrode and electrolyte potentials and concentrations are calculated to capture cell behavior. These models can explain internal dynamics of the cell, but that comes at the price of computational complexity. Therefore, electro-chemical models are most common in off-line simulations, where details on a low level are needed [6]. The most established electrochemical battery model is the model proposed by Doyle, Fuller, and Newman (DFN) [7].

3.2.2 Empirical Modeling

Empirical models, like the equivalent circuit model (ECM), aim to replicate the battery's current-voltage characteristics. However, these "grey-box" models have limited correlation with the physical reactions inside the cell. This limitation may restrict their applicability in non-equilibrium conditions, such as extreme temperatures and currents. Nevertheless, their simple structure allows for fast simulation and easier online parameter estimation compared to electrochemical models.

3.2.3 Data Driven Modeling

The data drive modeling alternatively called ads "black-box" modeling utilizes machine learning algorithms to learn relationships between battery input/output data and internal states (e.g., SoC, SoH). Black-box models can be very accurate with sufficient training data and can handle complex non-linear relationships. However, they may require significant computational resources.

3.3 Equivalent Circuit Modeling

The equivalent circuit model (ECM) uses electrical components such as resistors and capacitors to describe the relationship between current and voltage in a battery. There are several versions of the equivalent circuit model , in most cases, the model will be based on a circuit like the one in Figure 3.1 . Sometimes incorporating more RC pairs in series and sometimes non-linearities, such as hysteresis. The parameters in the models may be varying with SOC, temperature and current [6].

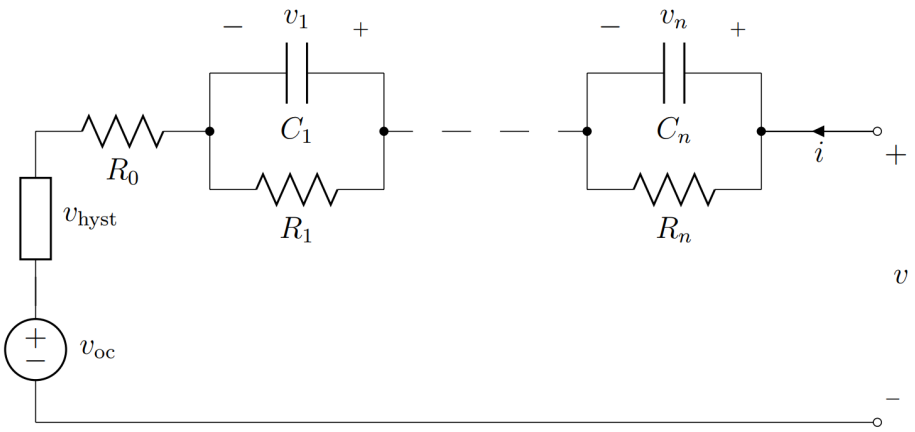

Figure 3.1: Thevenin Equivalent Circuit model with n-RC pairs and hysteresis

3.3.1 Open Circuit Voltage

The open circuit voltage is the equilibrium voltage of the cell. The OCV of a cell is then often defined as the potential difference between the anode and the cathode of a cell when it is at a resting state which means that there is no current flowing through it and that all transient effects have died out. [1]

At the full-cell level, the OCV vs. SoC curve is defined by the OCV curves of both active electrodes and two other significant parameters: the loading ratio that relates the capacity of the positive electrode (PE) with respect to the negative electrode(NE) and an offset that takes into consideration eventual SoC shifts between the electrodes, i.e. that an electrode might not be full when the other one is empty and vice versa, this is shown in Figure 3.2 [2]

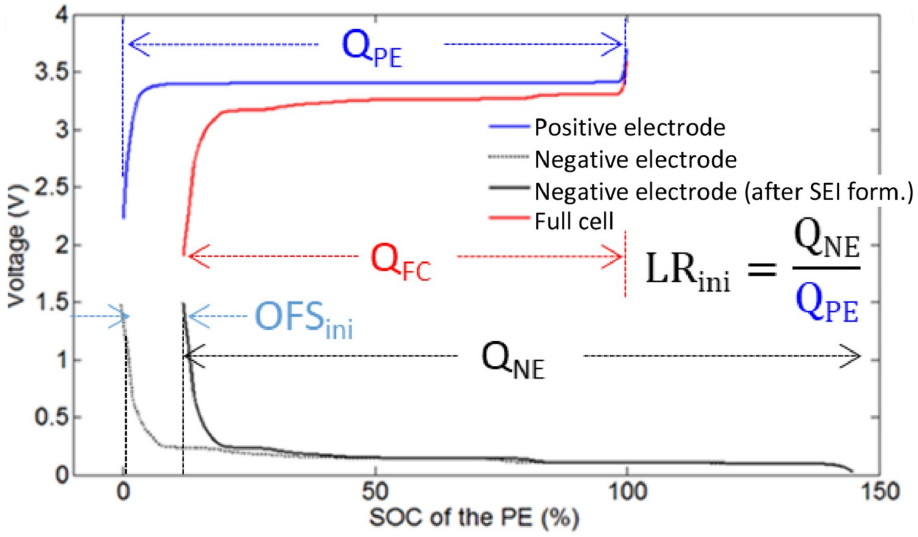

Figure 3.2: OCV relationship between full cell, PE and NE

The most common method of measuring the OCV vs. SoC curves is based on the galvanostatic intermittent titration technique (GITT) or pseudo-OCV test. One issue to measure the true OCV is that the voltage relaxation takes a long period of time to stabilize after load.

3.3.1.1 GITT Test

The Galvanostatic Intermittent Titration Technique (GITT) is a method used to characterize the electrochemical behavior of battery cells. In a typical GITT procedure, the cell is discharged or charged in small increments of State of Charge (SoC), followed by a rest period to allow for voltage relaxation. The process involves the following steps:

- **Incremental Discharge/Charge:** The cell is discharged or charged by a small percentage of its SoC, usually in steps of a few percent (e.g., 1-5%).
- **Rest Period:** After each incremental discharge or charge, the cell is allowed to rest for a period of a few hours.
- **Voltage Measurement:** The voltage response of the cell is recorded during the rest period. This relaxation behavior provides valuable insights into the cell's internal processes and kinetics.

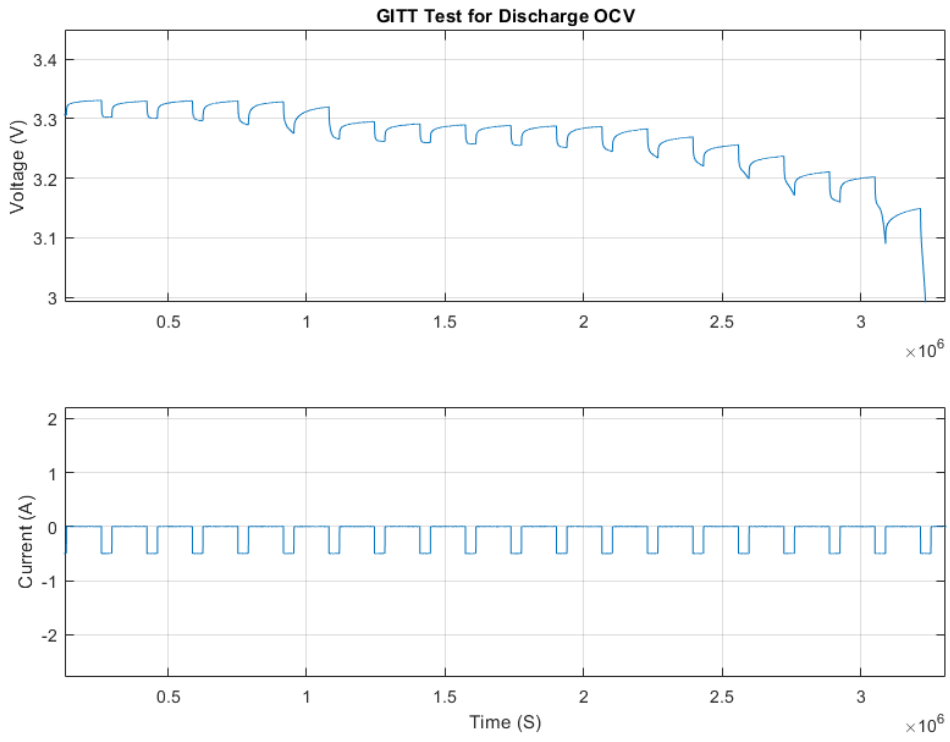

Figure 3.3: GITT test to extract discharge OCV

According to [3] , a cell with lithium iron phosphate (LFP) may not reach equilibrium even after 40 hours of rest. Conversely, [4] suggests that a rest period of 4 hours is sufficient for cells to approach a near-equilibrium state, where further

voltage changes are typically below the measurable threshold of 1 mV cannot be measured reliably.

While long relaxation periods can yield voltage values close to the theoretical equilibrium, one has to weigh the improvement of the measured values against the possibility of slow chemical reactions in the cell which alter the true equilibrium state. The authors of [4] proposed an optimal compromise between accuracy and duration by measuring the OCV for every 1% State of Charge (SoC) increment with a 4-hour rest period, resulting in a total test duration of approximately 17 days (101 rest periods). However, this extensive duration is often impractical and uneconomical for both academic and industrial researchers who may require faster results.

3.3.1.2 Pseudo OCV

An alternative to the Galvanostatic Intermittent Titration Technique (GITT) for obtaining Open Circuit Voltage (OCV) data involves using low-rate tests to average the charge and discharge curves, known as a pseudo-OCV profile. This method offers a practical balance between time efficiency and accuracy.

In this approach, the cell is charged and discharged at a very low rate, such as C/25, as demonstrated by Truchot et al. [5]. The process involves the following steps:

- **Low-Rate Charge and Discharge:** The cell is charged and discharged using a very low current, typically C/25, which minimizes polarization and allows the cell to approach its true OCV.
- **Averaging the Curves:** The charge and discharge voltage curves are averaged to derive a single-valued OCV profile. This averaged profile is used to represent the OCV at various State of Charge (SoC) levels.

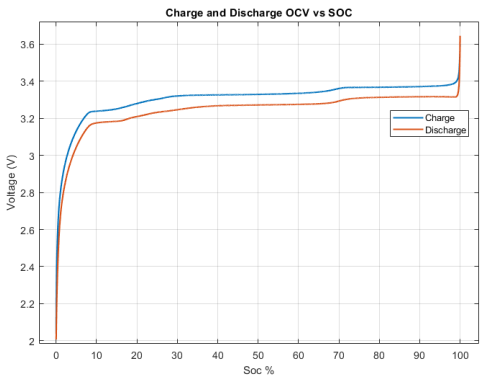

Figure 3.4: Ch & Dis OCV Curve

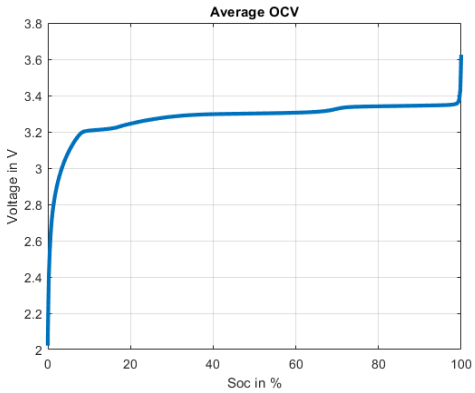

Figure 3.5: Average of Ch & Dis OCV

This pseudo-OCV profile provides a reliable approximation of the cell's OCV without the extensive rest periods required by GITT.

3.3.1.3 OCV Dependency on Temperature and SOH

According to the study by Bjorn Fridholm [6], the maximum observed voltage change was for a SoC of 20%, where the voltage difference was around 5 mV. This change corresponds to less than 0.5% in SoC, which was considered negligible. Therefore, while temperature does have an impact on the OCV, the effect is minimal and does not significantly affect the accuracy of SoC estimation under typical operating conditions. This observation can be seen in Figure 3.6

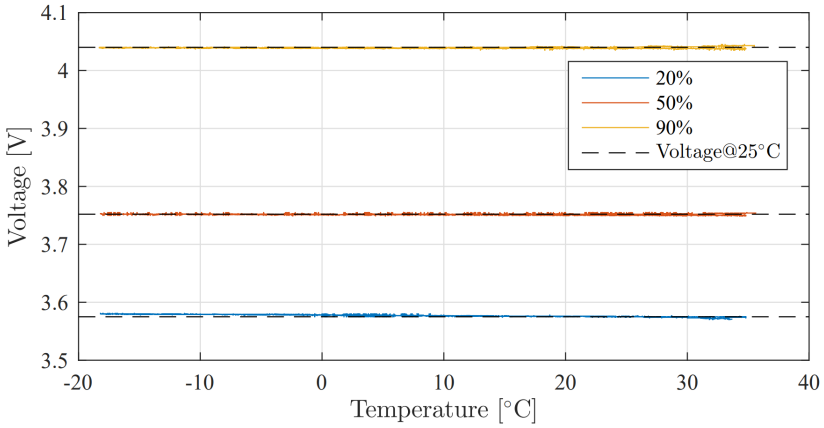

Figure 3.6: Voltage at constant SOC levels when sweeping the temperature of an NMC cell

In this study, State of Health (SoH) was not considered, and as such, the parameters, including the Open Circuit Voltage (OCV), are assumed to remain constant irrespective of the battery's SoH..

3.3.2 State of Charge and Capacity Estimation

State of Charge (SOC) is a key parameter that indicates the remaining charge in a battery, usually expressed as a percentage of the battery's full charge. Accurate SOC estimation involves several methodologies such as coulomb counting and OCV method.

- **Coulomb Counting Method:** This method involves integrating the current flowing in and out of the battery to estimate the SOC. It starts with a known initial SOC and updates based on the net charge transfer.
- **OCV Method:** The SOC is calculated from the OCV of the battery. Since the OCV Vs SOC curve can be established by laboratory tests, measuring the OCV allows for SOC estimation.

Capacity estimation determines the total charge a battery can hold, typically measured in ampere-hours (Ah). This parameter is crucial for evaluating battery health and predicting end-of-life. Capacity estimation techniques include:

- **Full Charge/Discharge Cycle::** Measuring the charge delivered during a full charge and discharge cycle to estimate capacity. Usually Constant cur-

rent(CC) is used in discharge capacity test and CC-CV method is used in charge capacity test.

- **Incremental Capacity Analysis (ICA):** Analyzing the differential change in capacity with respect to voltage to identify features indicative of battery capacity. It can identify capacity degradation trends without complete cycling.

3.3.3 Polarization

Polarization in the context of battery cells refers to the difference between the measured terminal voltage of the cell and the cell's internal open-circuit voltage (OCV) that arises due to the passage of electrical current. This phenomenon occurs because various internal processes within the battery create resistances and other effects that impact the voltage.

- **Activation Polarization**: This type of polarization represents the energy barrier that needs to be overcome for the electrochemical reactions at the electrode surfaces to occur. It's associated with the sluggish kinetics of the lithium-ion transfer process across the electrode-electrolyte interface. In simpler terms, it takes some initial energy to get the lithium ions moving between the electrodes.
- **Ohmic Polarization:** This results from the resistance to current flow within the battery itself. The resistance can arise from various sources, including:
  - **Electrolyte resistance**: The electrolyte solution has some inherent resistance to the movement of lithium ions.
  - **Electrode resistance**: The current needs to travel through the electrode materials, which also offer some resistance.
  - **Current collectors and tabs**: The metallic components that collect current from the electrodes also contribute a small amount of resistance.

  Ohmic polarization increases with higher discharge currents. As the current tries to flow through the battery faster, it encounters more resistance, leading to a larger voltage drop.
- **Concentration Polarization**: This type of polarization arises due to the uneven distribution of lithium ions within the electrodes during charge and discharge. As the battery operates, lithium ions are consumed or released near the electrode surfaces. This can lead to a concentration gradient within the electrode, where the concentration of lithium ions is higher near the current collector and lower closer to the separator. The diffusion of lithium ions within the electrode material tries to even out this concentration difference, but it takes time. The resulting concentration difference contributes to a voltage drop.

  It is more pronounced at higher discharge rates because the lithium ions don't have enough time to redistribute throughout the electrode material.

3.3.4 Modeling Voltage Polarization

The departure of the cell's terminal voltage away from OCV due to the passage of current can be modeled with different electrical circuits.

3.3.4.1 Rint Model

The cell's voltage drop is modeled as a resistance in series with the ideal voltage source(OCV). Cell voltage equals open circuit voltage as a function of state of charge minus the electrical current multiplied by R0. [8]

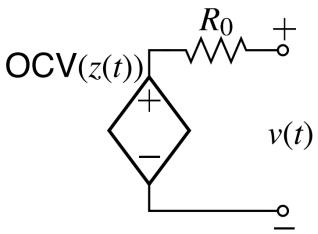

Figure 3.7: Simple Rint Model

$$v(t) = OCV(z(t)) - i(t) \times R_0$$

This models the instantaneous voltage response to a change in the input current. If electrical current is considered to have negative sign when charging and positive sign when discharging then voltage at the terminals of the cell is greater than the OCV when charging and less than the OCV at discharging. Even though it is quite simple, it is often good enough or sufficient as a basis for creating simple electronics designs for circuits that include battery cells. But when we're building a battery management system for an advanced consumer electronics application or a vehicle application where we require a really accurate model, this still is not accurate enough.

3.3.4.2 Thevenin Model

3.3.4.2.1 Diffusion Voltage The Rint model only models the instantaneous voltage response to a change in the input current. But in practice, we also observe a non instantaneous responses to change in input current. These are referred as dynamic responses. The battery cell's voltage will continue to evolve over time due to some previous change in input current. This is caused due to slow diffusion process in the cell.

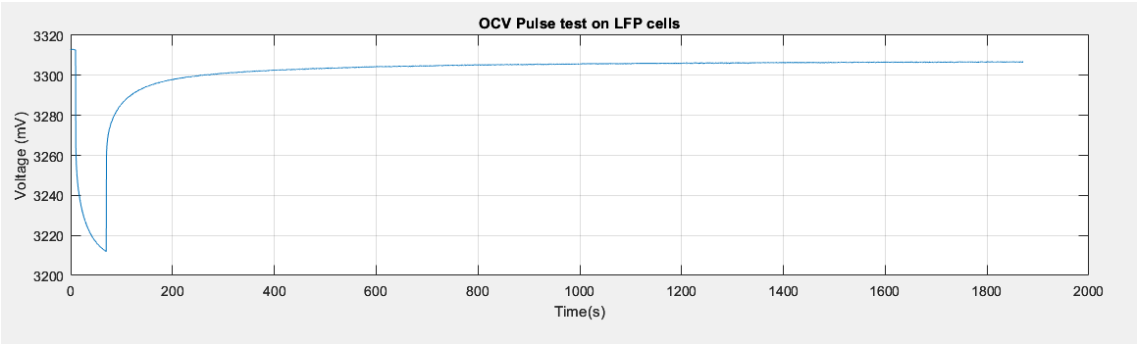

Figure 3.8: Response to a discharge pulse

Diffusion voltages can be closely approximated in a circuit using one or more parallel resistor-capacitor branch in series with the current path of the battery cell.

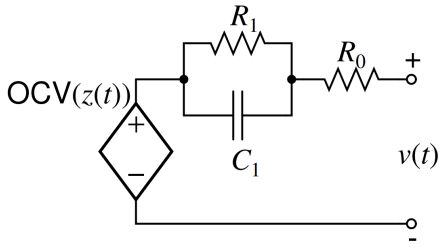

Figure 3.9: Thevenin Equivalent Circuit Model

$$v(t) = OCV(z(t)) - v_{C1}(t) - i(t) \times R_0$$

3.3.4.3 Randles Circuit

The Randles circuit is developed based on electro-chemical principles by understanding the internal operations of the battery. The Randles circuit has a resistance R_0 that models the electrolyte resistance. The R_{ct} is a charge transfer resistance that models the voltage drop across the interface between the electrode and the electrolyte. The C_{dl} is the double layer capacitance that models the effect of charge building up in the electrolyte near the electrode surface. And finally, the element Z_W is a warburg's impedance that models the slow diffusion process.

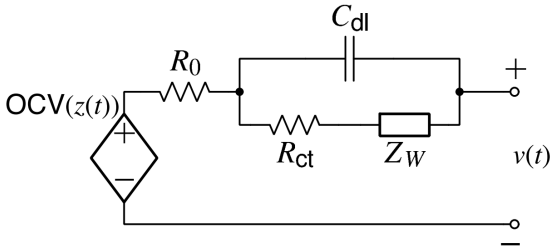

Figure 3.10: Randles Circuit

3.3.4.3.1 Modeling Warburg Impedance Z_W : No simple differential equation that we can write with standard calculus that represents a Warburg impedance exactly. But, it's possible to reproduce the effect of a Warburg impedance or approximate the effect using multiple resistor capacitor networks wired in series as shown in Figure 3.11 . We can approximate this impedance ZW using a parallel resistor capacitor branch with the values R1 and C1 in series with another parallel resistor capacitor branch R2 C2 and so forth. If we desire an exact perfect equivalence to the Warburg impedance, then we require an infinite number of resistor capacitor networks. But it turns out that the effect of Warburg impedance can often be modeled very well over some frequency range of interest using a relatively small number of resistor capacitor pairs.

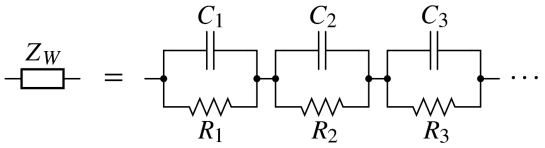

Figure 3.11: Warburg Impedance

The double layer capacitance is often omitted. It has negligible impact on the Randles circuit performance except at high frequencies. With C_{dl} removed from the circuit, R_0 and R_{ct} is combined, and Warburg impedance is replaced by a small finite number of R–C circuits, the model collapses to "Thévenin" model, with additional R–C pairs.

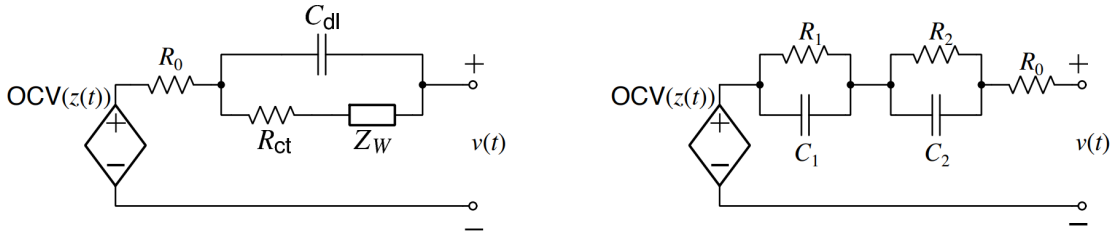

Figure 3.12: Randles Circuit reduced to Thevenin model with more RC pairs

3.3.5 Hysteresis Effect

In lithium-ion batteries, when a battery cell is allowed to rest for an extended period, the diffusion of voltages decays to zero, causing the model's voltage prediction to gradually converge to the open circuit voltage over time. However, in actual physical batteries,this is not the case. Instead, for each state of charge, there is a range of possible stable final voltages rather than a single stable final voltage. Ignoring the existence of this phenomenon will lead to very large state of charge prediction error risk.

For example in the Figure 3.13, suppose that you measured a cell voltage of 3.3 volts. According to this, 3.3 volts could correspond to any state of charge in between about 10% state of charge and about 95%. This wide range indicates that without accounting for this phenomenon, voltage measurements alone would not tell much information about the battery's SOC.

Hysteresis is a path-dependent voltage characteristic that does not decay to zero even when the cell is at rest. The change in hysteresis is directly related to the change in SOC rather than the change in time. [8]

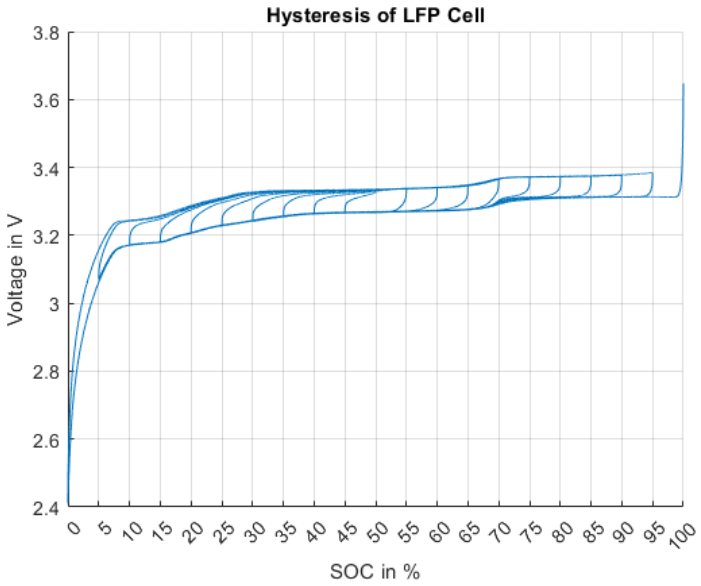

Figure 3.13: Hysteresis Effect in LFP Cells

4

Experimental Setup and Methodologies

The purpose of this chapter is to detail the experimental setup, including the methods used and the parameters controlled. Additionally, it describes the experiments conducted throughout the study. The results are analyzed in Chapter 5.

4.1 Experimental Equipment Set Up

4.1.1 Cell Specification

All tests were performed using a 10Ah LFP prismatic aluminum case cell provided by Hangzhou LIAO Technology Co., LTD.

Item	data（mm）
A	139
B	11
C	M6
D	7.5
E	15
F	65
G	14
H	36
I	7.5

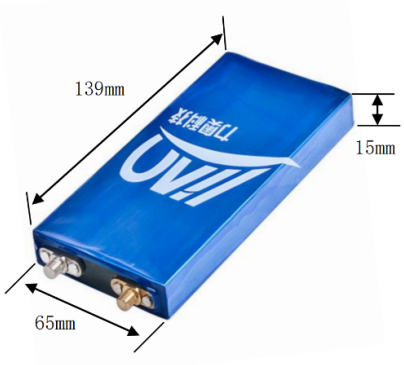

Image

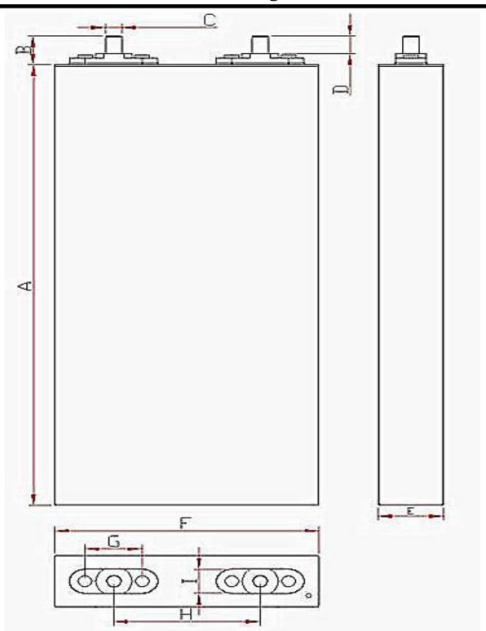

Figure 4.1: 10Ah LFP Cell Model No: F10-1565150

Item	Data	Remark
Size	150*65*15mm	L*W*H, including bolts
Nominal capacity	10Ah	25±5°C, 0.2C(2A), CC discharged to 2V
Nominal voltage	3.2V	
Charge cut-off voltage	3.65V	
Discharge cut-off voltage	2V	
Standard charge current	2A	0.2C CC to 3.65V, CV where I<200mA
Max. charge current	10A	1C(10A)
Standard discharge current	2A	0.2C(2A), CC discharged to 2V
Max continuous discharge current	30A	3C(30A), CC discharged to 2V
Weight	275±10g	
Charging Temp.	0 to 45°C	Suggested Temp.
Discharging Temp.	-20 to 60°C	Suggested Temp.

Table 4.1: Specifications of the LFP prismatic cell used in the tests

In this study, four cells (designated as Cell 1 through Cell 4) were examined, all sharing a common reference code: F10-1565150, originating from the same manufacturer. Various tests were conducted across these cells, with some experiments being conducted on multiple cells while others were solely performed on individual cells.

4.1.2 Cell Cycler

Figure 4.2: PEC CT0550 Battery Tester

The CT0550 is an 80-channel battery tester designed for high-volume tasks such as repetitive cycling, incoming goods inspection, and validation. It allows offline test preparation on a desktop PC via the LifeTest™ application, which communicates with the tester over Ethernet. Each channel is independent, utilizing POWER MOSFETs for high accuracy and flexibility, and the channels can be paralleled up to 1000 A.

- **Voltage/Current Specs:** 80 channels of 5V, 50A in one rack.
- **Additional I/O:** Optional analog and digital inputs/outputs through auxiliary I/O modules.
- **Load Types:** Supports current, voltage, power, and resistive loads with a minimum pulse width of 10 ms.
- **Switching Capabilities:** Ultra-fast switching between charging and discharging modes.

4.1.3 Thermal Chamber

Figure 4.3: Weiss Technik Reach-In Battery Test Thermal Chamber

The Weiss Technik reach-in battery test chambers are ideal for testing the reliability of battery cells and modules. These chambers can be configured with or without humidity control and come in sizes ranging from 7 to 54 cubic feet (190 to 1540 liters). They facilitate testing under a variety of conditions, including low or high temperatures, rapid temperature changes, and humidity.

- **Capacity:** Sizes from 7 to 54 cu. ft. (190 to 1540 liters).
- **Test Conditions:** Capable of simulating low/high temperatures, fast temperature changes, and humidity.
- **Purpose:** Designed for comprehensive testing of lithium batteries for reliability.

4.2 Equivalent Circuit Cell Modeling

4.2.1 Modeling SOC and Capacity

The cell is considered to be fully charged (Soc = 100%) when the cell OCV reaches the upper cut off voltage of 3.65V and fully discharged(Soc = 0%) when the cell OCV reaches the lower cut off voltage of 2V.

State of Charge is calculated using simple Coulomb counting. In discrete time, if we assume that the current is constant over the sampling interval $\triangle$t;

$$z[k+1] = z[k] - \frac{\triangle t \times \eta \times i[k]}{Q}$$

The Columbic efficiency η is assumed to be 1 for charge and discharge for simplicity.

The total capacity Q is defined as a the total amount of charge removed when discharging from Soc = 100% to Soc = 0%
Before conducting any other tests, a capacity test must be performed to estimate the state of charge (SOC) of the cells. This initial capacity test will serve as a calibration for the subsequent experiments. It is important to note that the rated capacity of a cell depends on various factors, including temperature, state of health (SOH), and the current rate. However, the capacity tests in this study will be performed using standardized reference parameters: a current rate of 0.2C and a temperature of 22.5°C. Throughout all tests, 1C current rate is defined as 10 A, although the actual capacity may slightly differ from 10 Ah.

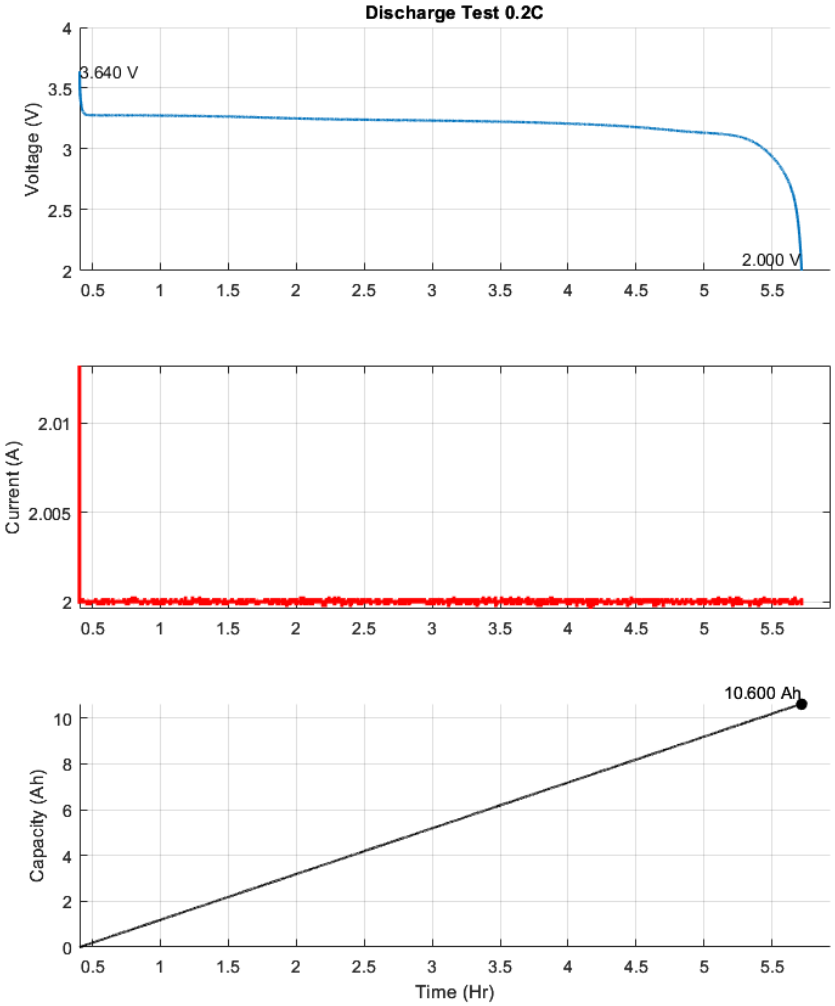

Figure 4.4: Discharging a fully charged LFP cell at 0.2 Crate

The test procedure to estimate the capacity of the cell:

1. CC charge battery to 3.65V with 2A.
2. CV charge battery at 3.65V until I $<$ 200mA.
3. CC discharge battery to 2V with 2A.

The total cell capacity, as determined through the discharge test, was approximately 10.6 Ah. This test was replicated on the remaining cells, and their capacities were found to be close to the mentioned value, exhibiting minimal variation around 10.6 Ah.

4.2.2 Modelling OCV vs SOC

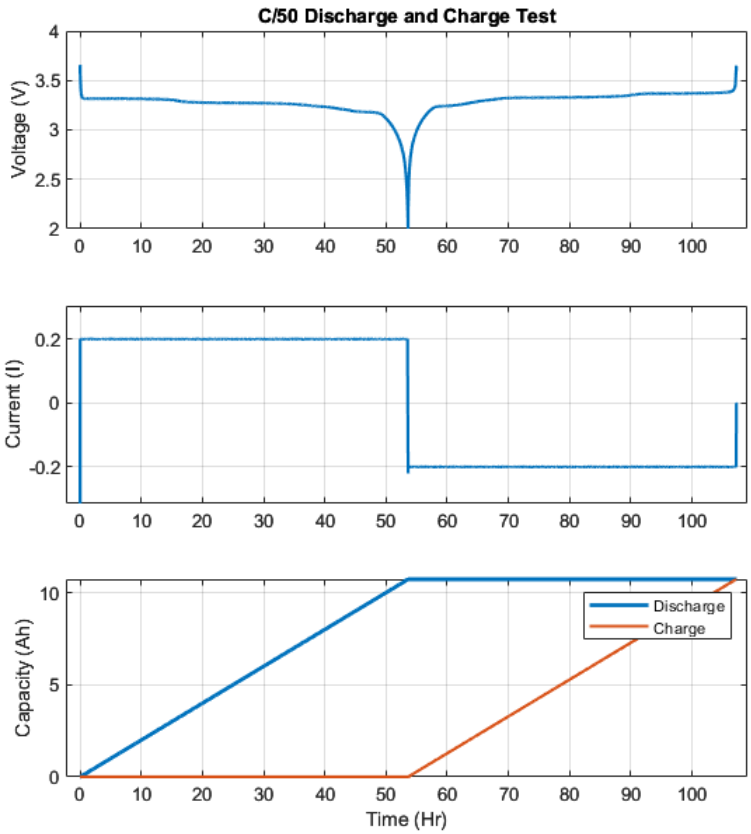

Figure 4.5: C/50 Discharging and Charging of LFP Cell

The following steps outline the procedure used to determine the average OCV :

1. CC discharge a fully charged battery to 3.65V with 0.2A(C/50) as shown in Figure 4.5.
2. CC charge an empty battery to 3.65V with 0.2A(C/50) as in Figure 4.5.
3. Find ohmic resistance R_0 at 0%, 25%, 50% ,75%, 100% for charge and discharge by measuring the instantaneous voltage change due to change in current and linearly interpolate for other SOCs. Table A.9
4. Subtract R_0 Resistance from charge & discharge OCV curve. This adjustment is clearly shown in Figure 4.7 which is a zoomed-in view of Figure 4.8
5. Average the charge and discharge OCV curve. The resultant average OCV is represented by the green line in Figure 4.8.

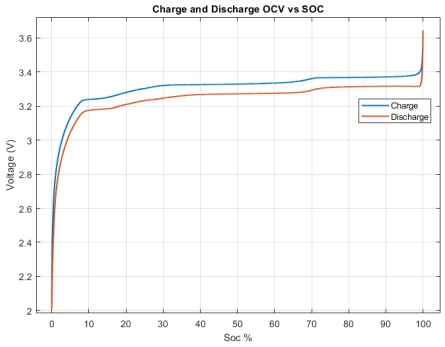

Figure 4.6: Ch & Dis OCV

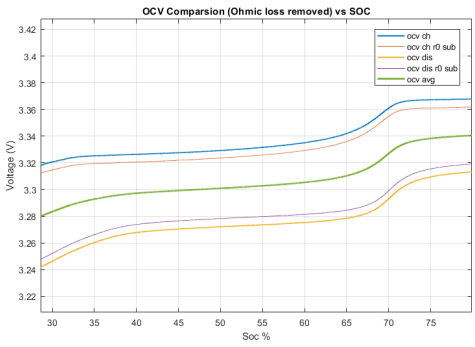

Figure 4.7: Zoomed in Version of 4.8

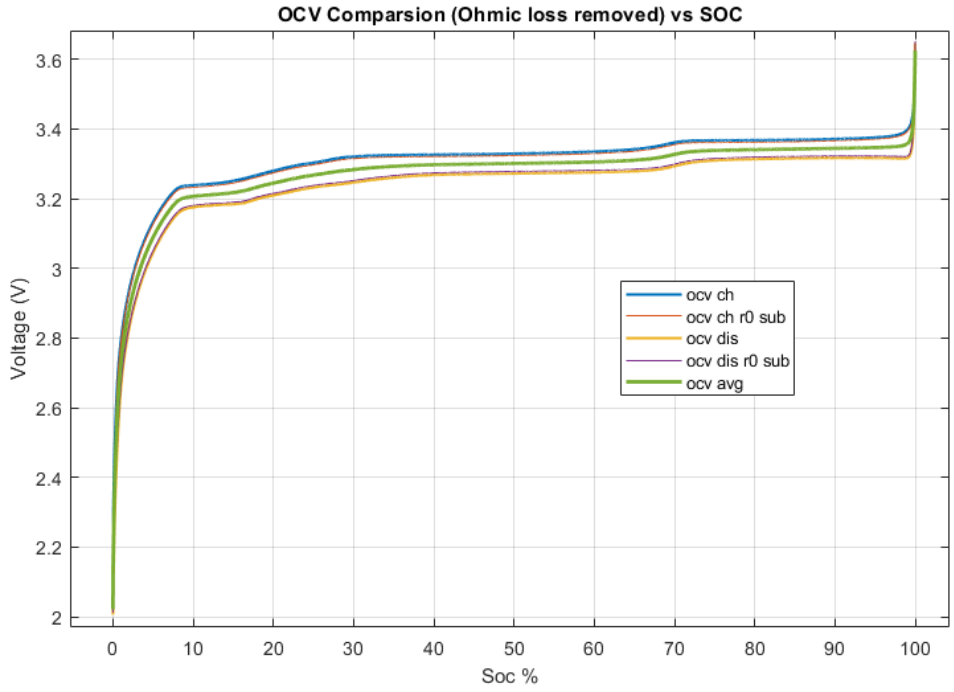

Figure 4.8: Averge OCV of LFP Cell

Table 4.2: SOC and Ohmic Resistances

SOC (%)	Charge Resistance R_0 (mV)	Discharge Resistance R_0 (mV)
0	6.4000	5.2000
25	6.0000	5.8000
50	5.6000	6.2000
75	6.2000	6.0000
100	4.6000	5.8000

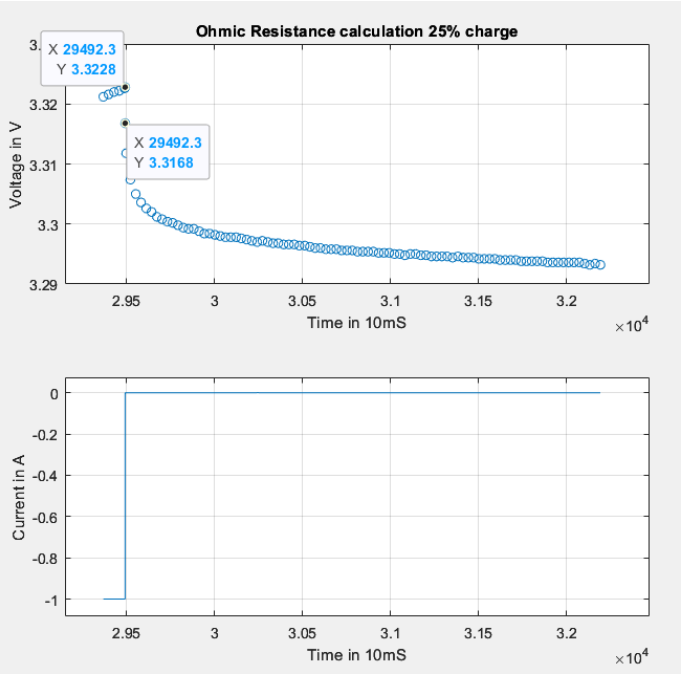

Figure 4.9: R_0 Resistance Calculated at 25% Soc by measuring change in voltage

4.2.3 Modeling Hysteresis

The test begins with a fully charged battery. The low current is used to ensure that the cell is nearly in equilibrium at every point of the test. Although this does not represent a completely true steady-state resting voltage, it is a close approximation.

Test procedure to collect the hysteresis data :

1. The cell is discharged at a rate of C/25 until it reaches the minimum voltage of 2.5 volts at 0% state of charge (SOC).
2. The cell is then charged at a rate of C/25 until it reaches 95% SOC. After reaching 95% SOC, the cell is discharged down to 5% SOC. The cell is charged up to 90% SOC and then discharged down to 10% SOC. This process is repeated, creating concentric loops of charging and discharging with progressively smaller SOC ranges over time.

By following this procedure, the hysteresis data is collected, capturing the behavior of the cell as it undergoes cycles of charging and discharging. See in Figure 4.10 and Figure 4.11
After collecting the data, the average open-circuit voltage (OCV) is subtracted from the recorded voltage data, as shown in Figure 4.12. The resulting difference represents the hysteresis voltage of the cell. Subsequently, a model based on Dr. Gregory Plett's hysteresis model is developed to describe the hysteresis voltage. [8]

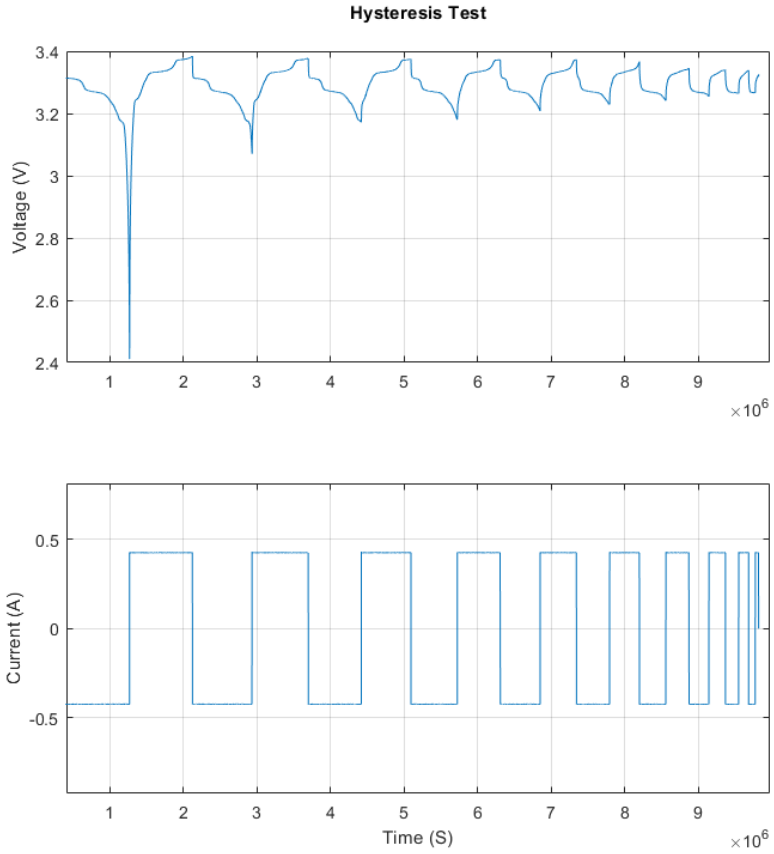

Figure 4.10: Cell Undergoes Cycles of Charging & Discharging

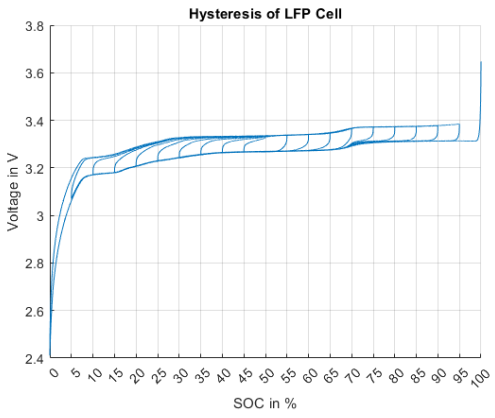

Figure 4.11: Ch & Dis OCV

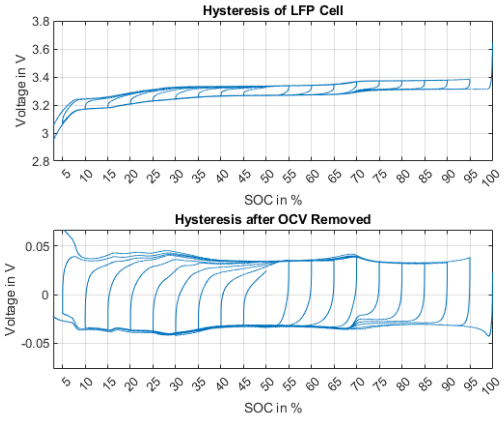

Figure 4.12: Zoomed in Version of 4.8

From Figure 4.12, we could see that there is a maximum positive and negative value of hysteresis at any state of charge. It is denoted as M(z). The value of hysteresis varies depending on whether the cell is being charged or discharged. Specifically, if the cell has been charging recently, the hysteresis value is positive, and if it has been discharging recently, the hysteresis value is negative.

This hysteresis envelope is influenced not only by the state of charge (SOC) but also by the recent charging or discharging activity. The sign of the input current indicates whether the cell is charging or discharging. Additionally, the sign of $\dot{z}$ the derivative of the state of charge with respect to time) also indicates the charging or discharging status.

To account for this effect, we modify M(z) to M(z, $\dot{z}$), incorporating the dependency on both the state of charge and the recent charging or discharging activity.

The hysteresis also changes in a manner that resembles resistor-capacitor (RC) decay. However, it is important to note that the hysteresis decays towards its maximum values when the state of charge (SOC) changes, rather than when time changes. This behavior suggests that hysteresis can be modeled as a differential equation, with the rate of change of the state of charge as a key factor.

$$\frac{dh(z,t)}{dz} = \gamma \operatorname{sgn}(\dot{z}) \left(M(z,\dot{z}) - h(z,t)\right) \tag{4.1}$$

- $\dot{z}$: Represents the rate of change of state of charge (SOC). It is positive for charging ($\dot{z} > 0$) and negative for discharging ($\dot{z} < 0$).
- $M(z,\dot{z})$: Denotes the maximum hysteresis, which is positive during charging and negative during discharging.
- $h(z,t)$: Represents the hysteresis voltage at a given state of charge z & time t.
- γ: A positive constant that tunes the rate of decay.
- sgn($\dot{z}$): The sign function, which indicates the direction of the rate of change of SOC, ensuring stability for both charging and discharging processes.

The term $M(z,\dot{z}) - h(z,t)$ causes the hysteresis rate of change to be proportional to the distance from the major hysteresis loop.

Multiplying both sides by $\frac{dz}{dt}$,

$$\frac{dh(z,t)}{dz}\frac{dz}{dt} = \gamma \operatorname{sgn}(\dot{z}) \left(M(z,\dot{z}) - h(z,t)\right) \frac{dz}{dt} \tag{4.2}$$

Left side becomes $\dot{h}(t)$; on right side, note $\dot{z}\operatorname{sgn}(\dot{z}) = |\dot{z}|$ and $\dot{z}(t) = -\eta(t)i(t)/Q$

$$\dot{h}(t) = -\left|\frac{\eta(t)i(t)\gamma}{Q}\right| h(t) + \left|\frac{\eta(t)i(t)\gamma}{Q}\right| M(z,\dot{z}) \tag{4.3}$$

Converting to discrete time assuming i(t) and $M(z,\dot{z})$ are constant over sampling period,

$$h[k+1] = \exp\left(-\frac{\eta[k]i[k]\gamma\Delta t}{Q}\right) h[k] + \left(1 - \exp\left(-\frac{\eta[k]i[k]\gamma\Delta t}{Q}\right)\right) M(z,\dot{z}) \tag{4.4}$$

where, $M(z,\dot{z}) = Msgn(i[k])$

The M(z, $\dot{z}$) is moved from the state equation to the output equation 4.7. Re-writing the above equation gives,

$$h[k+1] = \exp\left(-\frac{\eta[k]i[k]\gamma\Delta t}{Q}\right)h[k] - \left(1 - \exp\left(-\frac{\eta[k]i[k]\gamma\Delta t}{Q}\right)\right)\text{sgn}(i[k]) \quad (4.5)$$

$$u[k] = \begin{cases} \text{sgn}(i[k]), & |i[k]| > 0; \\ u[k-1], & \text{otherwise.} \end{cases}$$

$$h(k+1) = \alpha h(k-1) + (1-\alpha)u(k-1) \quad (4.6)$$

where, $\alpha = exp(-\frac{\eta i \triangle t \gamma}{Q})$, η is assumed to be 1 for charging and discharging

The hysteresis voltage comprises of two parts, one is instantaneous hysteresis and the other one is dynamic hysteresis. The instantaneous hysteresis changes when sign of current changes. You can see that in Figure 4.13, there is an immediate change in voltage when it moves from charging to discharging and vice versa. The dynamic hysteresis changes as SOC changes.
The hysteresis voltage is written as,

$$V_h(k) = M(z, \dot{z})[M_0 u(k) + (1 - M_0)h(k)] \quad (4.7)$$

where, $M_0 u(k)$ is instantaneous hysteresis and $(1 - M_0)$ is the remaining dynamic hysteresis

$$y(k) = M_0 u(k) + (1 - M_0)h(k) \quad (4.8)$$

where, y(k) = $\frac{V_h(k)}{M(z,\dot{z})}$

These equation are further written in input/output eqaution format to perform least square estimate and get the value of M_0

$$y(k) = \begin{bmatrix}\theta_1 & \theta_2 & \theta_3\end{bmatrix} \times \begin{bmatrix} y(k-1) \\ u(k) \\ u(k-1) \end{bmatrix} \quad (4.9)$$

where,
$\theta_1 = \alpha$
$\theta_2 = M_0$
$\theta_3 = (1 - \alpha - M_0)$

We could also see from the Figure 4.13, it takes 10% of Soc for the hysteresis voltage to move form discharge OCV to charge OCV but it only takes 5% of Soc to move the other way around. This suggest that the decay rate γ is different if you're going from charging to discharging or discharging to charging.

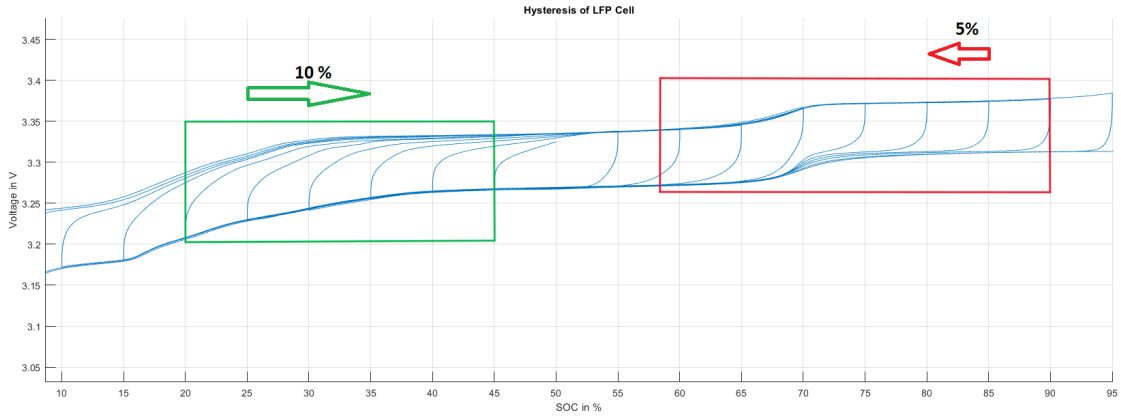

Figure 4.13: Hysteresis Test Procedure

Different gamma rates were selected to model the transitions between charge to discharge and discharge to charge. These rates were determined by iterating through a wide range of values and selecting the one that yielded the lowest Root Mean Square Error (RMSE).

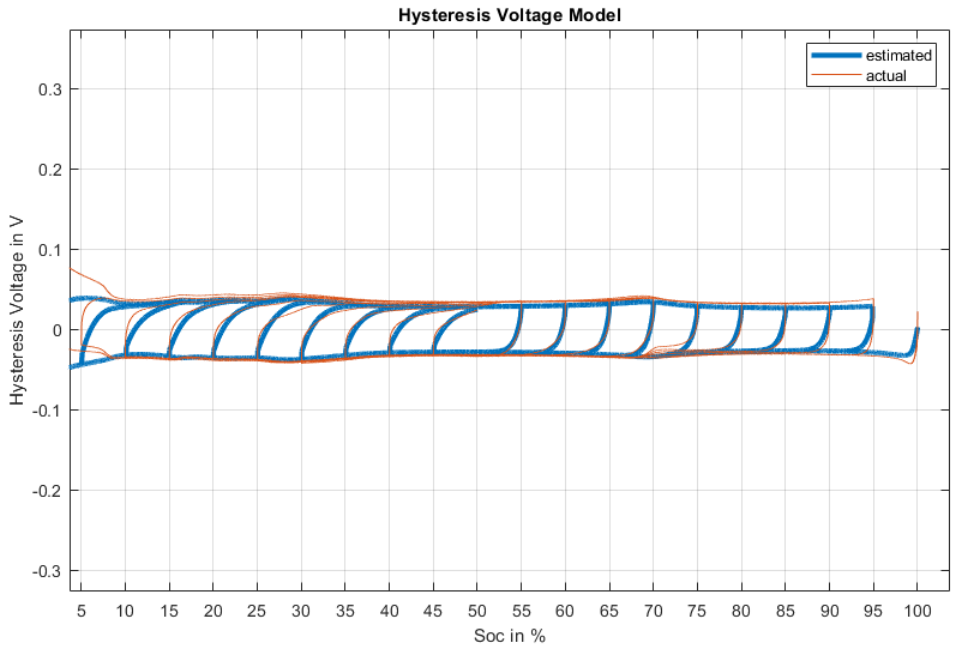

Figure 4.14: Hysteresis Voltage (Estimated Vs Actual)

4.2.4 ECM with 2 RC Pairs and Hysteresis

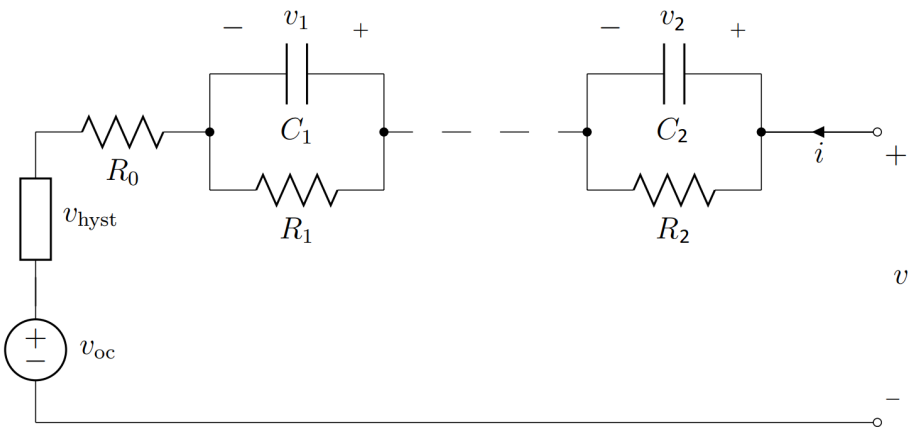

Figure 4.15: Thevenin Equivalent Circuit model with 2-RC pairs and hysteresis

By Kirchhoff's voltage law,

$$v = v_{oc}(z) + v_1 + v_2 + R_0 \cdot i + v_h \tag{4.10}$$

$$v - v_{oc}(z) - v_h = v_1 + v_2 + R_0 \cdot i \tag{4.11}$$

where $v - v_{oc}(z) - v_h = y$
In discrete form,

$$y(k) = v_1(k) + v_2(k) + R_o \cdot i(k) \tag{4.12}$$

$$v_1(k) = \alpha_1 \cdot v_1(k-1) + R_1 \cdot (1-\alpha_1) \cdot i(k-1) \tag{4.13a}$$

$$v_2(k) = \alpha_2 \cdot v_2(k-1) + R_2 \cdot (1-\alpha_2) \cdot i(k-1) \tag{4.13b}$$

where, $\alpha = exp(-\frac{i\triangle t}{Q})$
Substituting Eq.4.13a & 4.13b in Eq.4.12

$$y(k) = \alpha_1 \cdot v_1(k-1) + R_1 \cdot (1-\alpha_1) \cdot i(k-1) + \alpha_2 \cdot v_2(k-1) + R_2 \cdot (1-\alpha_2) \cdot i(k-1) + R_o \cdot i(k) \tag{4.14}$$

These equation are further solved and written in input/output equation format to perform least square estimate and get the value of the unknowns

$$y(k) = \left(\frac{\alpha_1^2 \cdot \alpha_2}{\alpha_2 - \alpha_1} + \frac{\alpha_2^2 \cdot \alpha_1}{\alpha_1 - \alpha_2}\right) \cdot y(k-2) + \left(\frac{\alpha_1^2}{\alpha_1 - \alpha_2} - \frac{\alpha_2^2}{\alpha_1 - \alpha_2}\right) \cdot y(k-1) + \left(\frac{\alpha_2^2 - \alpha_1^2}{\alpha_1 - \alpha_2} \cdot (R_1 \cdot (1-\alpha_1) + R_2 \cdot (1-\alpha_2)) + \frac{\alpha_1^2 \cdot \alpha_2 - \alpha_2^2 \cdot \alpha_1}{\alpha_1 - \alpha_2} \cdot R_0 + \alpha_1 \cdot R_1 \cdot (1-\alpha_1) + \alpha_2 \cdot R_2 \cdot (1-\alpha_2)\right) \cdot i(k-2) + \left(\frac{\alpha_1^2 \cdot R_0 - \alpha_2^2 \cdot R_0}{\alpha_2 - \alpha_1} + R_1 \cdot (1-\alpha_1) + R_2 \cdot (1-\alpha_2)\right) \cdot i(k-1) + R_0 \cdot i(k) \tag{4.15}$$

$$y(k) = \begin{bmatrix} \theta_1 & \theta_2 & \theta_3 & \theta_4 & \theta_5 \end{bmatrix} \times \begin{bmatrix} y(k-1) \\ y(k-2) \\ i(k) \\ i(k-1) \\ i(k-2) \end{bmatrix} \tag{4.16}$$

where,

$$\theta_1 = \left(\frac{\alpha_1^2}{\alpha_1 - \alpha_2} - \frac{\alpha_2^2}{\alpha_1 - \alpha_2}\right) = \alpha 1 + \alpha 2$$

$$\theta_2 = \left(\frac{\alpha_1^2 \cdot \alpha_2}{\alpha_2 - \alpha_1} + \frac{\alpha_2^2 \cdot \alpha_1}{\alpha_1 - \alpha_2}\right) = -\alpha 1 \cdot \alpha 2$$

$$\theta_3 = R_0$$

$$\theta_4 = \left(\frac{\alpha_1^2 \cdot R_0 - \alpha_2^2 \cdot R_0}{\alpha_2 - \alpha_1} + R_1 \cdot (1-\alpha_1) + R_2 \cdot (1-\alpha_2)\right)$$

$$\theta_5 = \left(\frac{(\alpha_2^2 - \alpha_1^2 \cdot (R_1 \cdot (1-\alpha_1) + R_2 \cdot (1-\alpha_2)) + (\alpha_1^2 \cdot \alpha_2 - \alpha_2^2 \cdot \alpha_1) \cdot R_0}{\alpha_1 - \alpha_2} + \alpha_1 \cdot R_1 \cdot (1-\alpha_1) + \alpha_2 \cdot R_2 \cdot (1-\alpha_2)\right)$$

Rearranging $\theta 1$ and $\theta 2$,

$$\alpha 2 = \theta 1 - \alpha 1 \tag{4.17a}$$

$$\alpha 2 = \frac{-\theta 2}{\alpha 1} \tag{4.17b}$$

Equating the above 2 equations and solving for $\alpha 1$,

$$\alpha 1 = \frac{\theta 1}{2} \pm \sqrt{\left(\frac{\theta 1}{2}\right)^2 + \theta 2} \tag{4.18}$$

Finding R_1 and R_2,

$$\begin{bmatrix} \theta_4 \\ \theta_5 \end{bmatrix} = \begin{bmatrix} -(\alpha 1 + \alpha 2) \\ \alpha 1 \cdot \alpha 2 \end{bmatrix} \cdot R_0 + \begin{bmatrix} 1 - \alpha 1 & 1 - \alpha 2 \\ -\alpha 2(1-\alpha 1) & \alpha 1(1-\alpha 2) \end{bmatrix} \cdot \begin{bmatrix} R_1 \\ R_2 \end{bmatrix} \tag{4.19}$$

$$\begin{bmatrix} R_1 \\ R_2 \end{bmatrix} = A^{-1} \left(\begin{bmatrix} \theta_4 \\ \theta_5 \end{bmatrix} - B \cdot R_0 \right) \tag{4.20}$$

where C_1 and C_2 are ,

$$C_1 = \frac{5}{R_1} \tag{4.21}$$

$$C_2 = \frac{40}{R_2} \tag{4.22}$$

4.2.5 Root Mean Squared Error

In this study, the Root Mean Square Error (RMSE) was used to quantify the error between the measured voltage V_{meas} and the calculated voltage V_{calc}. The RMSE is defined as:

$$\text{RMSE} = \sqrt{\frac{1}{N}\sum_{i=1}^{N}\left(V_{\text{meas},i} - V_{\text{calc},i}\right)^2}$$

where N is the number of data points, $V_{\text{meas},i}$ is the measured voltage at the i-th data point, and $V_{\text{calc},i}$ is the calculated voltage at the i-th data point. The RMSE provides a measure of the magnitude of the error, with lower values indicating better accuracy.

4.2.6 Flowchart of parameter identification process

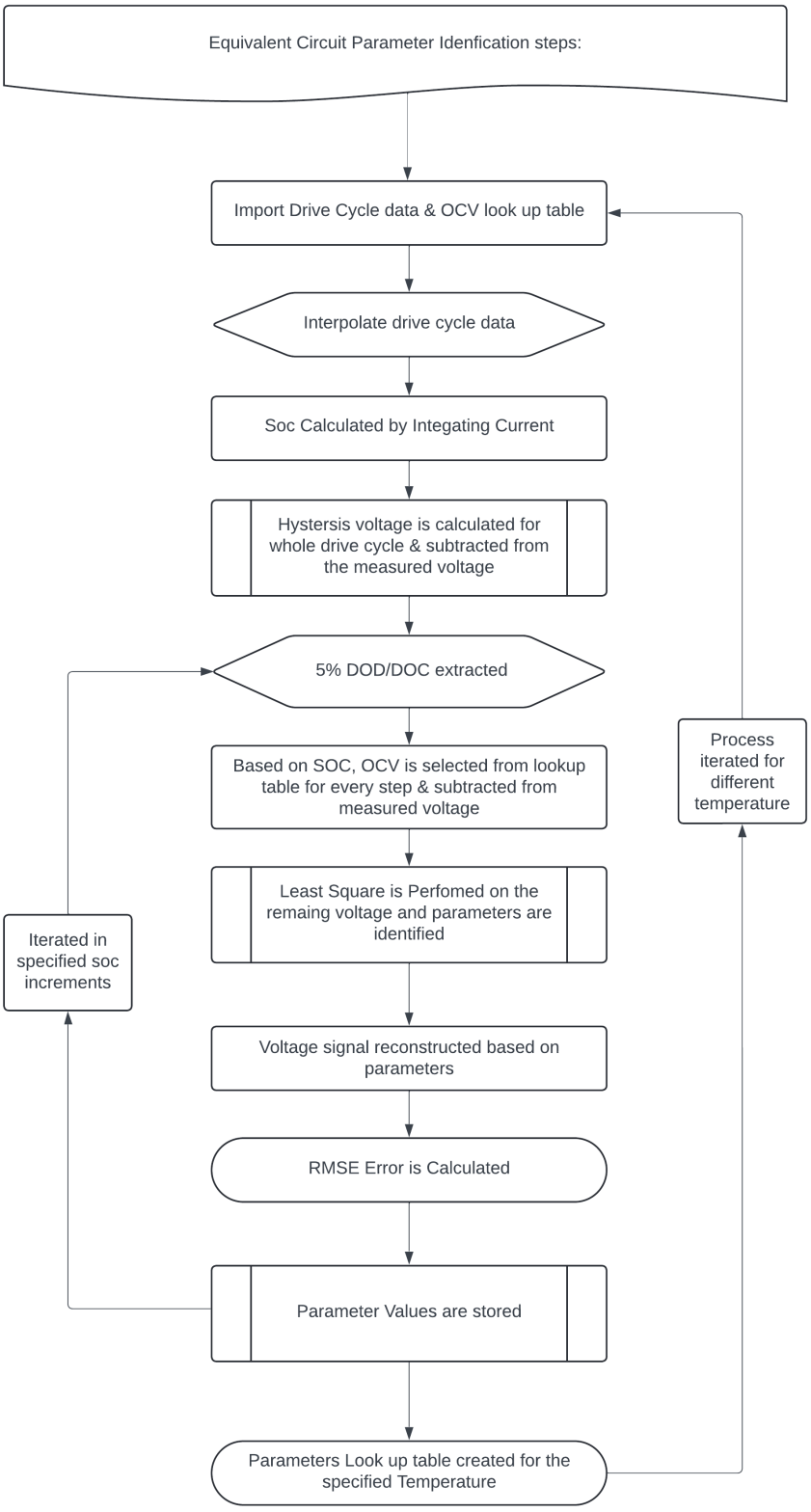

Figure 4.16: Step by step overview of the identification process

5

Results

5.1 ECM with 2RC Verification with Synthetic Data

To verify the model, synthetic data was generated using the voltage equation with predefined parameters R_0, R_1, R_2, C_1, and C_2. The current was fed as an input to this equation, and the resulting voltage response was captured. This captured voltage response was then provided to the least squares estimation model, which calculated the parameters. The estimated parameters matched exactly with the predefined values, as the synthetic data was generated without any disturbances. Two tests were conducted: one with a current pulse input and another with a random current input. In both tests, the model successfully identified the parameters accurately.

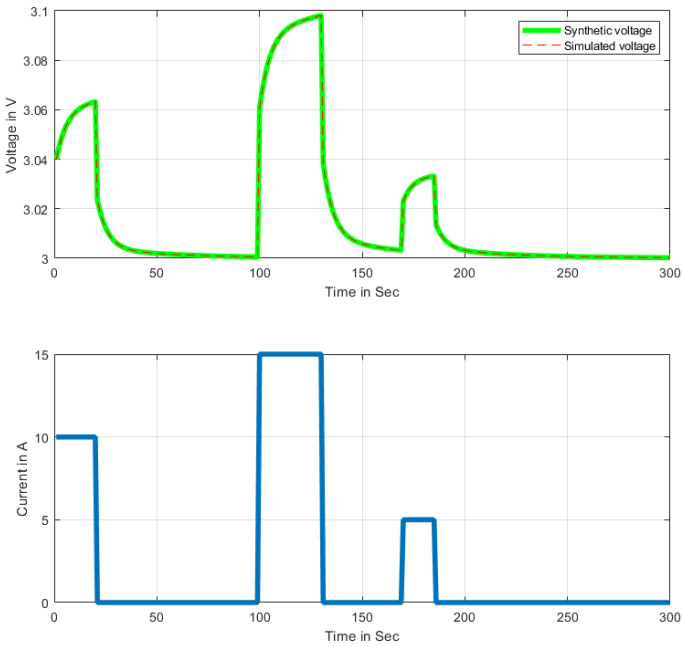

Figure 5.1: Voltage Response to Current Pulse

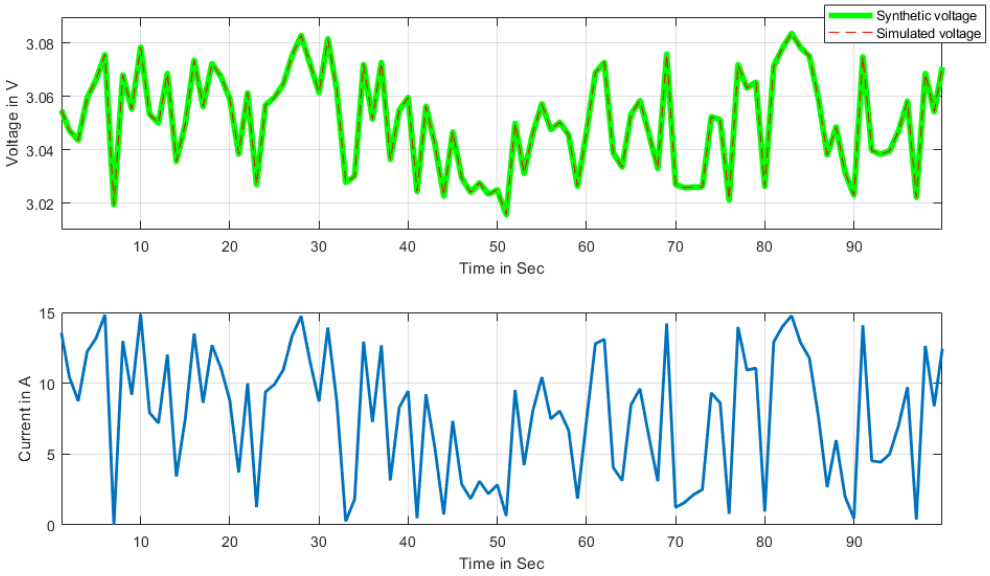

Figure 5.2: Voltage Response to Given Current Input

5.2 ECM Parameter Analysis for Discharge Pulses Across Different C-Rates

This discharge test was conducted to provide an initial input for the model by feeding the discharge pulse data. The objective was to evaluate how accurately the model predicts the voltage response for a given input current. To assess the performance of the model, the least square error between the measured and simulated voltage was calculated. Additionally, these tests offer insights into how well the model captures the effects of different C-rates on ECM parameters.

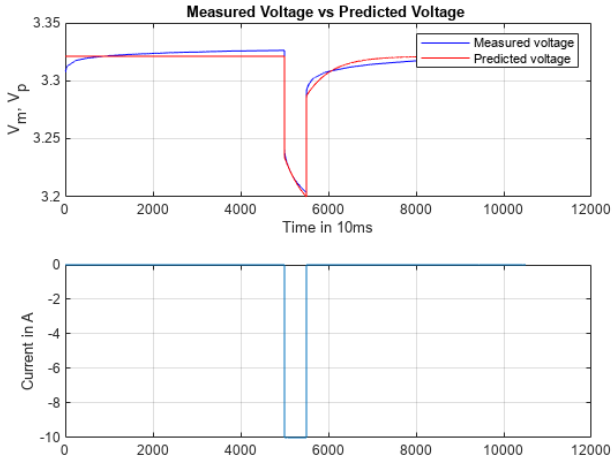


```
Section Soc Range for current Discharge test
   79.7417
   79.6097
Predicted Values:
R0_hat = 8.2270e-03 Ohm
R1_hat = 4.8736e-04 Ohm
R2_hat = 6.1161e-03 Ohm
C1_hat = 1.0259e+04 F
C2_hat = 6.5401e+03 F
RMSE for the LSE :
    0.0038
```

Figure 5.3: ECM Parameters at 80% 1C Discharge

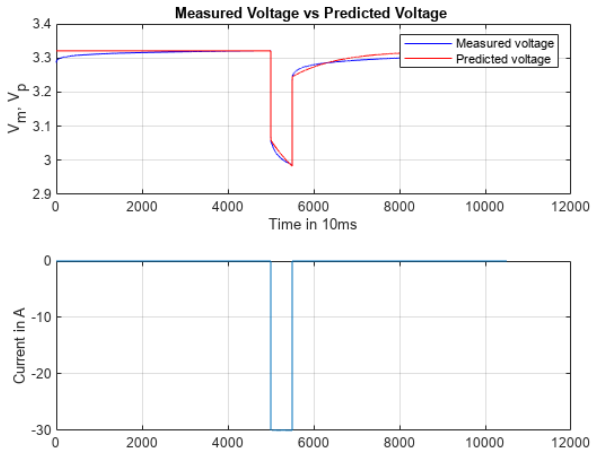


```
Section Soc Range for current Discharge test
   79.6097
   79.2229
Predicted Values:
R0_hat = 8.1137e-03 Ohm
R1_hat = 6.0061e-04 Ohm
R2_hat = 6.8015e-03 Ohm
C1_hat = 8.3249e+03 F
C2_hat = 5.8811e+03 F
RMSE for the LSE :
    0.0101
```

Figure 5.4: ECM Parameters at 80% 3C Discharge

5.3 ECM Parameters based on Drive Cycles

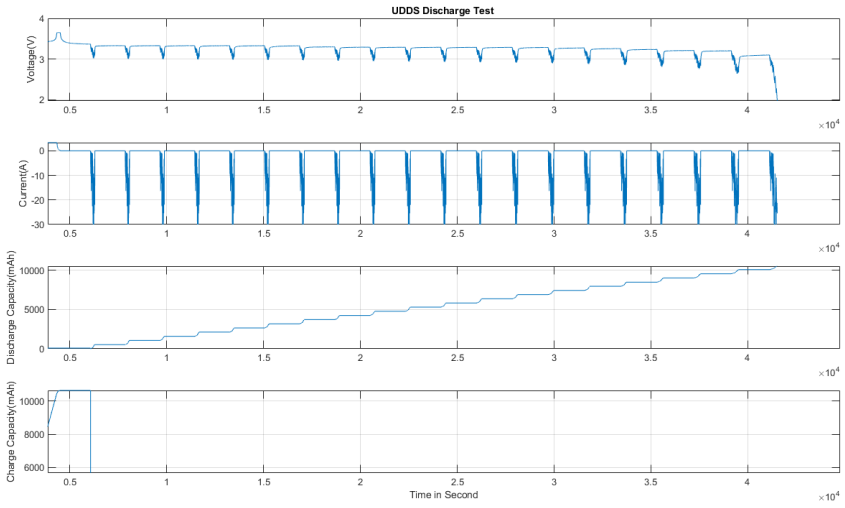

Figure 5.5: UDDS Drive Cycle Discharge Test $T = 22\,^{\circ}\mathrm{C}$

A UDDS drive cycle with a discharge and charge current profile was used to capture the voltage response of the cell. The drive cycle was executed at a 5% depth of

discharge (DOD), with the cell being discharged or charged and then rested for a specified period. After each resting phase, the same current profile was applied again. This process was repeated until the cell reached the minimum voltage (V_{min}) during discharge and the maximum voltage (V_{max}) during charging. Additionally, the entire process was performed at different temperatures to evaluate the impact of temperature on the battery's performance and parameter identification.

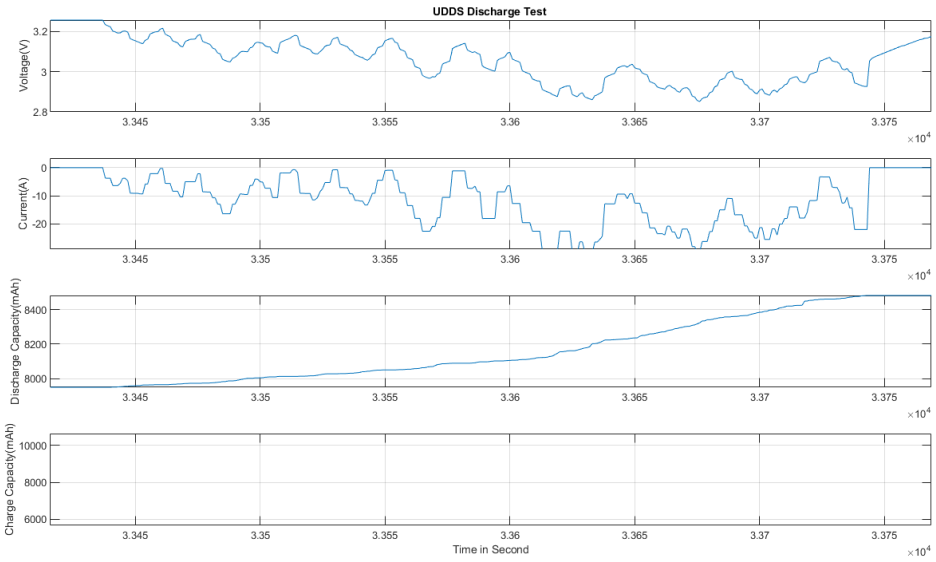

Figure 5.6: Zoomed in Version of 5.5

The current profile utilized in the tests is derived from the Urban Dynamometer Driving Schedule (UDDS) drive cycle. The velocity profiles from the UDDS are converted into a current profile, which is then scaled down to match the maximum discharge current of the battery. This scaling ensures that the current profile aligns with the battery's capabilities, preventing over-stressing the cell during the tests and maintaining the integrity of the measurements.

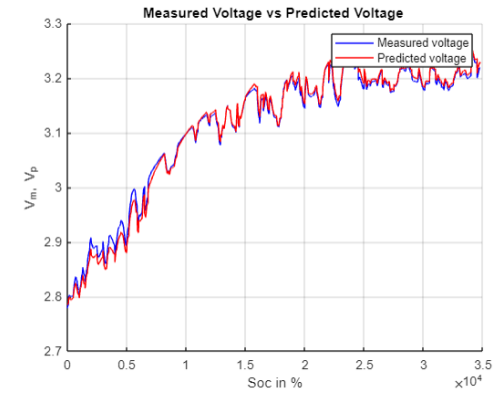


```
Section Soc Range for current Discharge test
    6.1982
   11.1982
Predicted Values:
R0_hat = 6.8754e-03 Ohm
R1_hat = 7.2621e-06 Ohm
R2_hat = 5.0126e-03 Ohm
C1_hat = 6.8851e+05 F
C2_hat = 7.9798e+03 F
RMSE for the LSE :
    0.0078
```

Figure 5.7: ECM Parameters at 5% Discharge and $T = 30\,°\mathrm{C}$

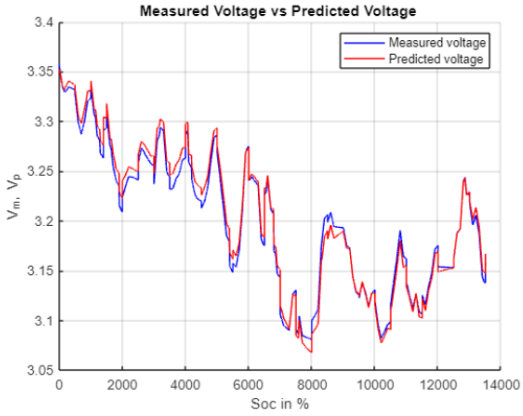


```
Section Soc Range for current Discharge test
   94.4763
   89.4763
Predicted Values:
R0_hat = 5.2179e-03 Ohm
R1_hat = 2.9990e-05 Ohm
R2_hat = 4.0925e-03 Ohm
C1_hat = 1.6672e+05 F
C2_hat = 9.7740e+03 F
RMSE for the LSE :
    0.0064
```

Figure 5.8: ECM Parameters at 95% Discharge and $T = 30\,°\mathrm{C}$

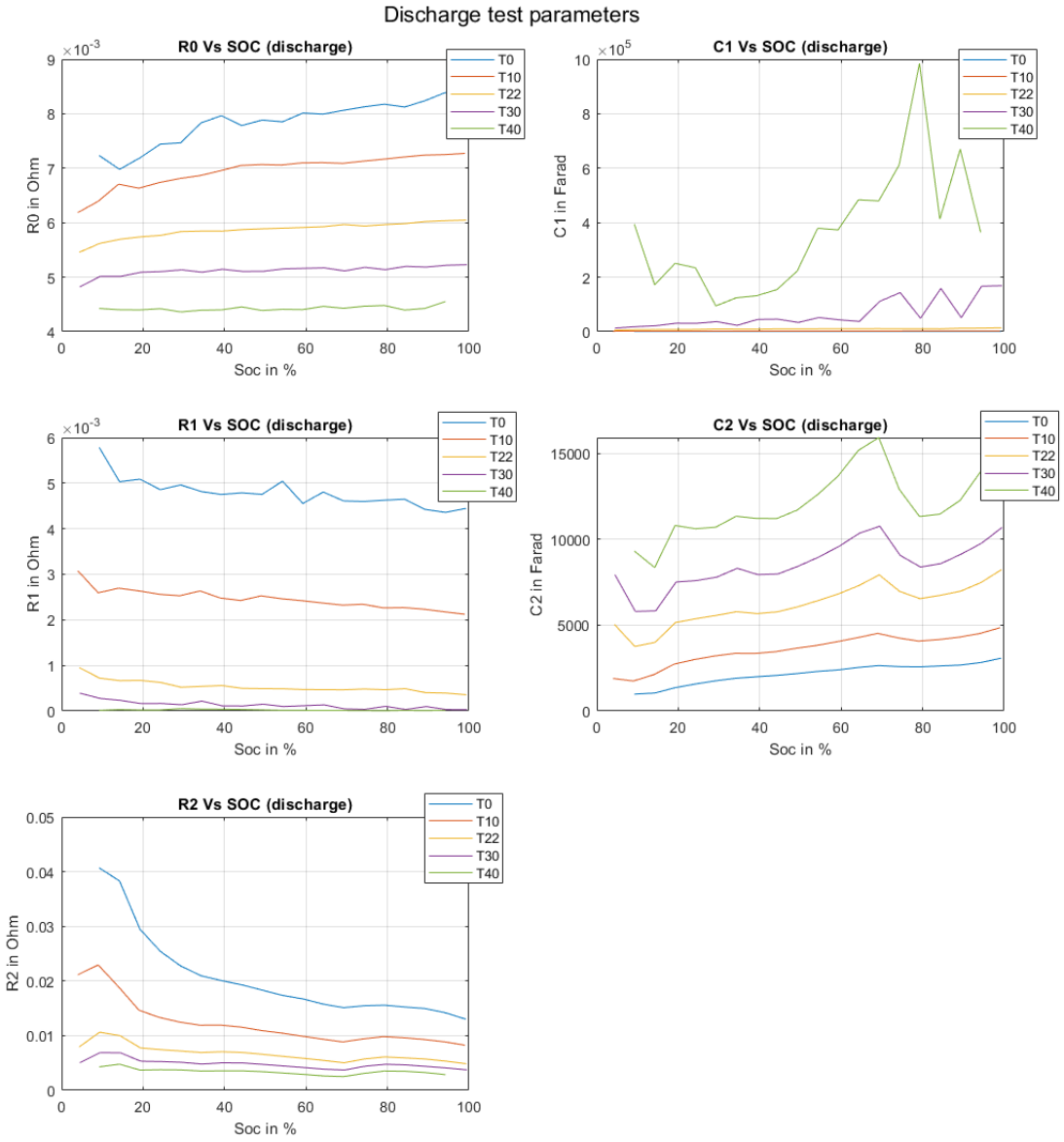

Figure 5.9: ECM Parameters for Discharge Test

In the discharge tests, the ohmic resistance (R_0) was observed to increase as the temperature decreased, following the trend from $T = 40°C$ to $T = 30°C$, $T = 22°C$, $T = 10°C$, and $T = 0°C$. Additionally, a slight increase in R_0 values was noted at SOC levels close to 100%. Similarly, the values for R_1 and R_2 exhibited an increasing trend as the temperature was lowered. This consistent observation of higher resistance at decreasing temperatures aligns with the expected behavior of battery materials.

In contrast, the capacitance parameters (C_1 and C_2) showed an inverse relationship with temperature. These parameters had higher values at elevated temperatures

and lower values as the temperature decreased, which is the opposite trend to that of the resistance values.

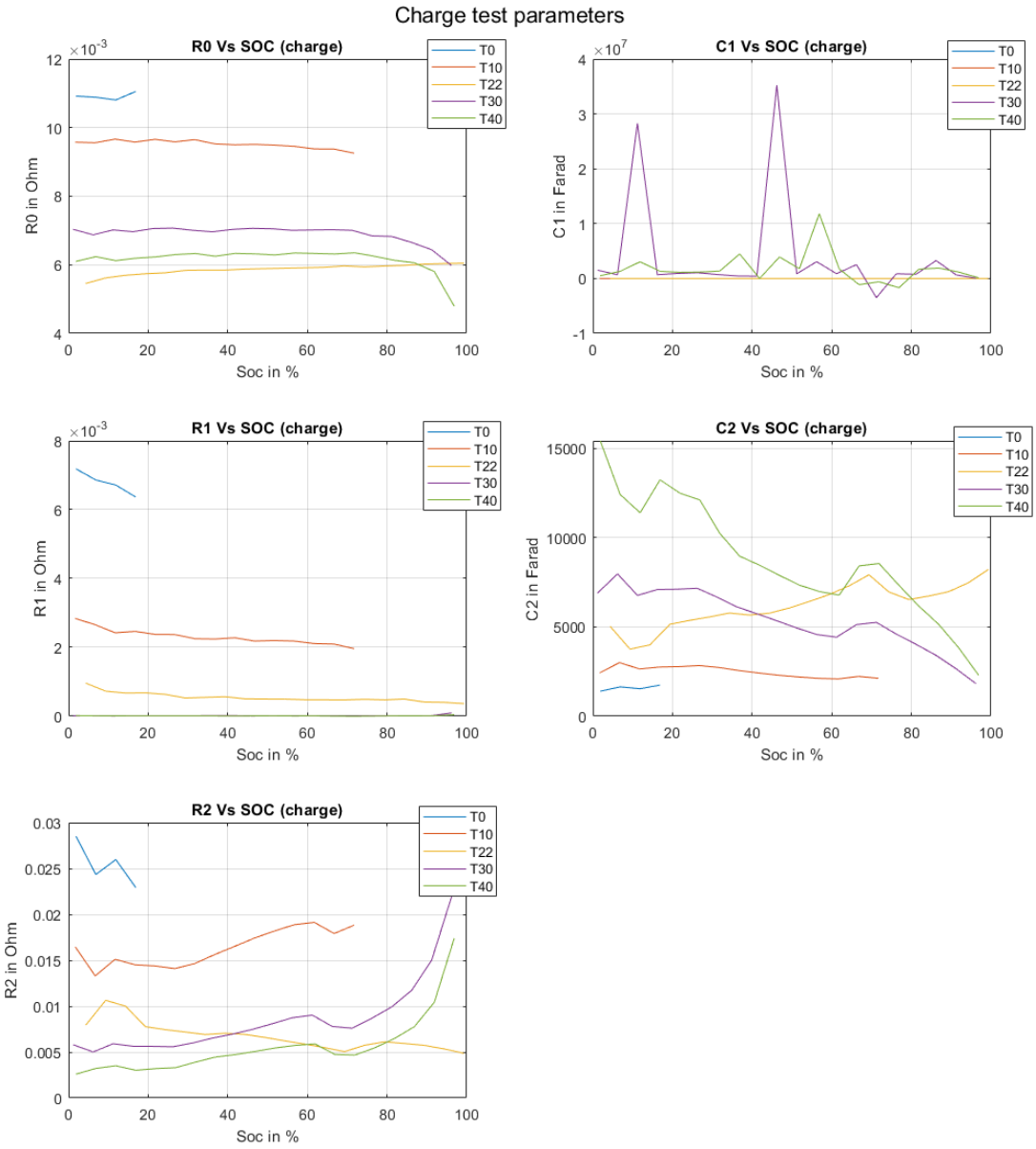

Figure 5.10: ECM Parameters for Charge Test

In the charging drive cycles, some identified parameters, such as R_1 and C_1, yielded negative values, which are physically unrealistic. This anomaly can be attributed to inaccuracies in the predicted Open Circuit Voltage (OCV). The residual voltage, calculated as the difference between the terminal voltage and the OCV ($V_{\text{residual}} = V_{\text{terminal}} - V_{\text{OCV}}$), occasionally resulted in incorrect inputs to the model. Specifically, in certain cases, the OCV used was higher than the terminal voltage, leading to

negative residual voltage and subsequently causing the model to output negative parameter values.
The OCV curve used in this analysis was established using a C/30 test, which may not provide sufficient resolution for highly accurate OCV estimation since the current is not completely zero when recording the data. Other method, such as the Galvanostatic Intermittent Titration Technique (GITT), could potentially yield more precise OCV values. Employing such a method might have prevented the occurrence of negative parameter values by minimizing errors in OCV estimation, thereby improving the overall reliability of the identified model parameters.

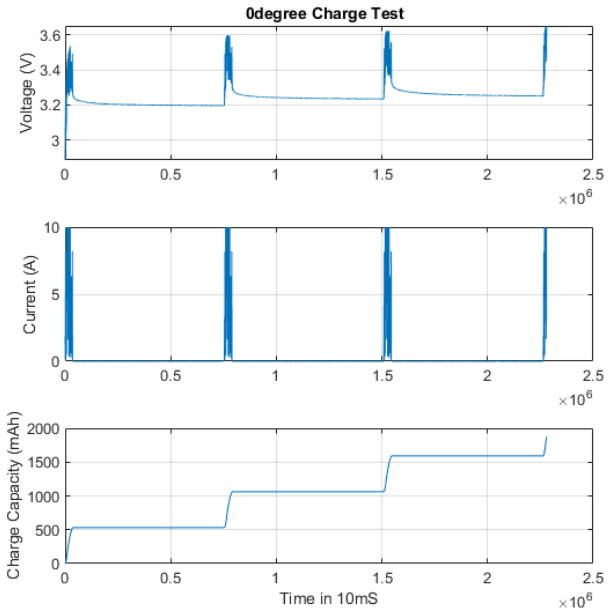

Figure 5.11: Charge $T = 0\,°C$

The lookup table data at $T = 0\,°C$ (5.1) is limited to 20% SOC. During the charge tests, the cell voltage reached the upper cut-off voltage prematurely. This is due to the high internal resistance encountered at low temperatures, which accelerates the voltage rise. Similarly, for the test conducted at $T = 10\,°C$, the lookup table data extends only up to 80% SOC. The higher internal resistance at this temperature also led to an earlier attainment of the upper cut-off voltage.

Table 5.1: UDDS Charge Test $T = 0\,°C$

SOC_{Start}	SOC_{End}	R_0 (ohm)	R_1 (ohm)	R_2 (ohm)	C_1 (F)	C_2 (F)	RMSE
1.86	6.87	0.0109	7.1860e-03	0.02853	695.8	1402.2	0.0362
6.87	11.87	0.0109	6.8601e-03	0.02433	728.9	1643.7	0.0330
11.87	16.87	0.0108	6.7137e-03	0.02598	744.7	1539.6	0.0336
16.87	19.58	0.0111	6.3656e-03	0.02294	785.5	1744.0	0.0319

5.4 Validation

The parameters were validated using the Urban Dynamometer Driving Schedule (UDDS) drive cycle, which includes both charge and discharge profiles. First, Hysteresis voltage and OCV was calculated throughout the entire test and subtracted from the measured voltage. The remaining voltage is given as an input to the model. Specifically, the charge parameters were utilized to calculate the charge current, while the discharge parameters were applied to determine the discharge profiles. The selection of these parameters was tailored to the operating temperature and State of Charge (SOC) range, ensuring that the parameters are appropriate for the specific conditions under which the battery operates.

The Root Mean Square Error (RMSE) between the measured voltage and the voltage calculated using the Equivalent Circuit Model (ECM) parameters was found to be 0.0234. While this RMSE is slightly higher than desired, it points to potential areas for improvement in the model or the measurement process. Several factors could contribute to this discrepancy:

1. **Open Circuit Voltage (OCV) Estimation**: Accurate OCV estimation is crucial for reliable model predictions. Any errors in OCV estimation directly affect the accuracy of the ECM. The OCV-SOC relationship may have been inadequately characterized, leading to inaccuracies, especially if the battery's true OCV varies significantly from the estimated values under certain conditions.
2. **Parameter Sensitivity**: ECM parameters, such as resistance and capacitance, are highly sensitive to operating conditions, including temperature and SOC. Variability or slight inaccuracies in these parameters can result in significant deviations between measured and calculated voltages.
3. **Model Limitations**: The ECM, while effective, simplifies the battery's complex behavior into resistive and capacitive elements. This simplification might not fully capture transient dynamics or non-linearities in battery behavior, contributing to higher RMSE in certain scenarios.
4. **Measurement Noise and Errors**: The accuracy of the voltage measurements themselves could affect the RMSE. Noise in the measurement data or errors introduced by the instrumentation can also lead to discrepancies between the measured and calculated voltages.
5. **Drive Cycle Characteristics**: The UDDS drive cycle, used for validation, includes a range of operational scenarios (acceleration, cruising, and braking). Variations in current profiles during these scenarios might not be perfectly captured by the ECM, especially during rapid transitions.

Despite these challenges, the RMSE of 0.0234 indicates that the model provides a reasonable approximation of the battery's behavior under typical operating conditions. Continuous refinement of the OCV estimation and ECM parameters, along with enhanced measurement accuracy, could further reduce this error, leading to more precise voltage predictions.

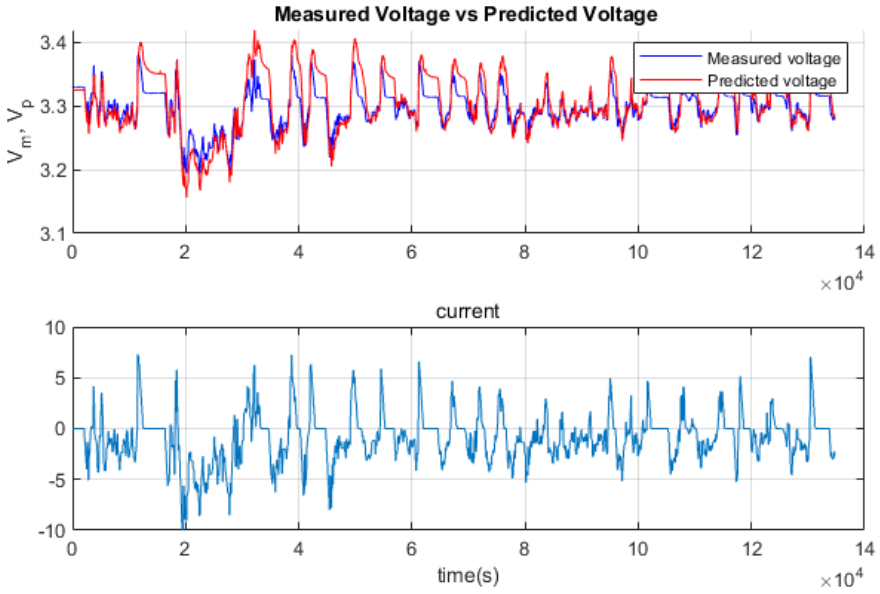

Figure 5.12: UDDS Drive Cycle Parameter Validation

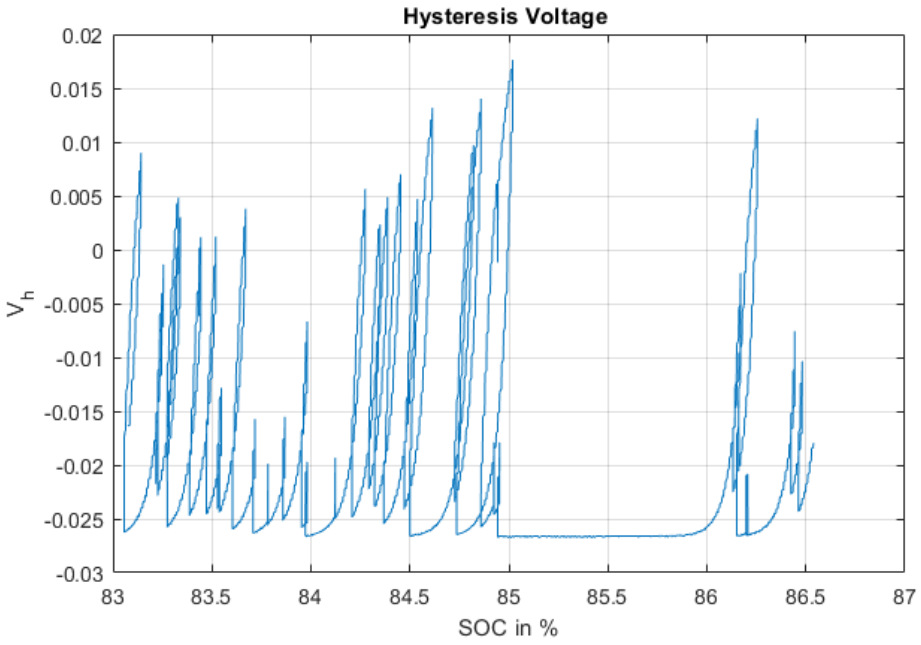

Figure 5.13: Hysteresis voltage for above Figure 5.12

6
Conclusion

This thesis developed a robust method for identifying equivalent circuit model (ECM) parameters for lithium-ion batteries under various conditions. By employing realistic drive cycle profiles and accounting for temperature and hysteresis effects, the method produced parameter sets that reliably captured battery behavior across a range of SOCs and temperatures. The results demonstrated the increasing trend of resistances at lower temperatures and the inverse behavior of capacitive elements, highlighting the impact of temperature on battery dynamics.

Model verification using synthetic data confirmed the accuracy of the parameter estimation process, with the model successfully recovering predefined parameters for both pulse and random current inputs. However, challenges such as inaccuracies in open circuit voltage (OCV) estimation below 0°C affected parameter reliability in some cases. Refining the OCV determination process, possibly through methods like GITT, could further enhance the model's precision.

This work lays the groundwork for integrating accurate ECM parameters into advanced battery management systems (BMS), offering significant potential for improving state estimation and battery performance predictions in automotive and other applications. Future efforts could address OCV estimation challenges and extend the framework to incorporate aging effects for long-term applicability.

Bibliography

[1] Larrat, G. (2023). Open-Circuit-Voltage hysteresis measurement and modelling of LiFePO4 Batteries: Master Thesis Report-2023.

[2] Dubarry, M., Truchot, C., Liaw, B. Y. (2012). Synthesize battery degradation modes via a diagnostic and prognostic model. Journal of power sources, 219, 204-216.

[3] Kindermann, F. M., Noel, A., Erhard, S. V., & Jossen, A. (2015). Long-term equalization effects in Li-ion batteries due to local state of charge inhomogeneities and their impact on impedance measurements. Electrochimica Acta, 185, 107-116.

[4] Barai, A., Chouchelamane, G. H., Guo, Y., McGordon, A., & Jennings, P. (2015). A study on the impact of lithium-ion cell relaxation on electrochemical impedance spectroscopy. Journal of Power Sources, 280, 74-80.

[5] Truchot, C., Dubarry, M., & Liaw, B. Y. (2014). State-of-charge estimation and uncertainty for lithium-ion battery strings. Applied Energy, 119, 218-227.

[6] Fridholm, B. (2019). Adaptive Model-Based Battery Management: Predicting Energy and Power Capability. Chalmers Tekniska Hogskola (Sweden).

[7] Doyle, M., & Newman, J. (1995). The use of mathematical modeling in the design of lithium/polymer battery systems. Electrochimica Acta, 40(13-14), 2191-2196.

[8] Plett, G. L. (2015). Battery management systems, Volume I: Battery modeling. Artech House.

A

Appendix

A.1 Discharge and Charge Parameters at Different Temperatures

Table A.1: UDDS Discharge Test $T = 0\,^{\circ}\mathrm{C}$

SOC_{Start}	SOC_{End}	R_0 (ohm)	R_1 (ohm)	R_2 (ohm)	C_1 (F)	C_2 (F)	RMSE
99.24	94.23	0.008302	0.004445	0.013019	1124.77	3072.50	0.0506
94.23	89.23	0.008390	0.004359	0.014187	1146.96	2819.56	0.0509
89.23	84.23	0.008240	0.004424	0.014965	1130.24	2672.82	0.0538
84.23	79.23	0.008124	0.004649	0.015245	1075.61	2623.80	0.0553
79.23	74.23	0.008176	0.004626	0.015574	1080.81	2568.45	0.0556
74.23	69.23	0.008127	0.004598	0.015475	1087.33	2584.89	0.0581
69.23	64.23	0.008064	0.004610	0.015120	1084.67	2645.45	0.0541
64.23	59.23	0.007993	0.004805	0.015768	1040.54	2536.74	0.0565
59.23	54.23	0.008014	0.004555	0.016725	1097.78	2391.63	0.0594
54.23	49.23	0.007852	0.005044	0.017367	991.22	2303.19	0.0612
49.23	44.23	0.007884	0.004754	0.018335	1051.71	2181.65	0.0621
44.23	39.23	0.007783	0.004788	0.019309	1044.31	2071.60	0.0636
39.23	34.23	0.007965	0.004752	0.020073	1052.14	1992.70	0.0631
34.23	29.23	0.007832	0.004816	0.020965	1038.11	1907.98	0.0627
29.23	24.23	0.007466	0.004963	0.022743	1007.52	1758.77	0.0634
24.23	19.23	0.007442	0.004857	0.025438	1029.44	1572.48	0.0655
19.23	14.23	0.007190	0.005088	0.029483	982.63	1356.73	0.0700
14.23	9.23	0.006979	0.005032	0.038297	993.62	1044.48	0.0722

Table A.2: UDDS Disharge Test $T = 10\,°C$

SOC_{Start}	SOC_{End}	R_0 (ohm)	R_1 (ohm)	R_2 (ohm)	C_1 (F)	C_2 (F)	RMSE
98.99	93.99	0.007272	0.002122	0.008251	2355.76	4847.61	0.0248
93.99	88.99	0.007249	0.002177	0.008872	2297.10	4508.37	0.0238
88.99	83.99	0.007240	0.002233	0.009303	2238.86	4299.69	0.0249
83.99	78.99	0.007205	0.002269	0.009617	2203.39	4159.22	0.0256
78.99	73.99	0.007166	0.002263	0.009828	2209.71	4070.18	0.0261
73.99	68.99	0.007129	0.002342	0.009401	2134.70	4254.92	0.0261
68.99	63.99	0.007089	0.002323	0.008853	2152.20	4518.00	0.0233
63.99	58.99	0.007103	0.002370	0.009371	2109.63	4268.66	0.0252
58.99	53.99	0.007098	0.002421	0.009913	2065.34	4035.12	0.0264
53.99	48.99	0.007059	0.002463	0.010479	2029.85	3817.10	0.0274
48.99	43.99	0.007068	0.002526	0.010945	1979.16	3654.63	0.0281
43.99	38.99	0.007051	0.002425	0.011581	2061.87	3454.08	0.0291
38.99	33.99	0.006954	0.002478	0.011930	2017.84	3352.88	0.0295
33.99	28.99	0.006865	0.002635	0.011915	1897.59	3357.19	0.0291
28.99	23.99	0.006811	0.002528	0.012483	1977.58	3204.26	0.0295
23.99	18.99	0.006737	0.002562	0.013343	1951.93	2997.93	0.0314
18.99	13.99	0.006633	0.002635	0.014663	1897.20	2727.91	0.0339
13.99	8.99	0.006708	0.002696	0.018928	1854.46	2113.31	0.0383
4.33	0.19	0.00546	0.000953	0.00794	5247.80	5039.28	0.0334

Table A.3: UDDS Disharge Test $T = 22\,°C$

SOC_{Start}	SOC_{End}	R_0 (ohm)	R_1 (ohm)	R_2 (ohm)	C_1 (F)	C_2 (F)	RMSE
99.34	94.33	0.0060	0.000355	0.00486	14065.95	8230.25	0.0110
94.33	89.33	0.0060	0.000393	0.00535	12719.44	7482.96	0.0095
89.33	84.33	0.0060	0.000403	0.00573	12402.43	6979.42	0.0104
84.33	79.33	0.0060	0.000490	0.00594	10203.51	6738.17	0.0110
79.33	74.33	0.00596	0.000467	0.00612	10714.11	6540.97	0.0115
74.33	69.33	0.00594	0.000483	0.00574	10360.39	6967.16	0.0119
69.33	64.33	0.00597	0.000465	0.00504	10743.76	7929.17	0.0119
64.33	59.33	0.00593	0.000468	0.00548	10688.66	7302.23	0.0112
59.33	54.33	0.00591	0.000471	0.00587	10623.46	6819.68	0.0116
54.33	49.33	0.00590	0.000488	0.00622	10252.18	6429.66	0.0124
49.33	44.33	0.00589	0.000490	0.00659	10194.41	6066.49	0.0129
44.33	39.33	0.00587	0.000497	0.00693	10065.65	5773.75	0.0133
39.33	34.33	0.00585	0.000558	0.00705	8954.66	5670.38	0.0132
34.33	29.33	0.00585	0.000540	0.00691	9259.01	5784.72	0.0137
29.33	24.33	0.00584	0.000521	0.00719	9590.44	5566.53	0.0143
24.33	19.33	0.00577	0.000626	0.00744	7983.16	5374.78	0.0145
19.33	14.33	0.00574	0.000672	0.00777	7443.49	5150.56	0.0159
14.33	9.33	0.00570	0.000665	0.01000	7518.39	4000.14	0.0195
9.33	4.33	0.00562	0.000720	0.01064	6940.72	3760.12	0.0196
4.33	0.19	0.00546	0.000953	0.00794	5247.80	5039.28	0.0334

Table A.4: UDDS Disharge Test $T = 30\,°C$

SOC_{Start}	SOC_{End}	R_0 (ohm)	R_1 (ohm)	R_2 (ohm)	C_1 (F)	C_2 (F)	RMSE
99.49	94.48	0.005229	2.9653e-05	0.003743	168616.60	10687.92	0.0086
94.48	89.48	0.005218	2.9990e-05	0.004092	166719.86	9773.99	0.0064
89.48	84.48	0.005185	9.7489e-05	0.004378	51288.07	9135.59	0.0070
84.48	79.48	0.005198	3.1522e-05	0.004659	158618.49	8584.99	0.0074
79.48	74.48	0.005138	1.02098e-04	0.004772	48972.66	8382.48	0.0080
74.48	69.48	0.005181	3.4891e-05	0.004414	143301.90	9062.86	0.0086
69.48	64.48	0.005115	4.5039e-05	0.003717	111015.87	10762.38	0.0108
64.48	59.48	0.005171	1.3384e-04	0.003864	37358.50	10352.93	0.0075
59.48	54.48	0.005162	1.1524e-04	0.004172	43389.58	9587.36	0.0075
54.48	49.48	0.005152	9.6797e-05	0.004462	51654.75	8965.39	0.0079
49.48	44.48	0.005107	1.4890e-04	0.004742	33578.80	8434.82	0.0083
44.48	39.48	0.005105	1.0946e-04	0.005013	45679.20	7978.89	0.0090
39.48	34.48	0.005145	1.1154e-04	0.005035	44826.54	7943.66	0.0091
34.48	29.48	0.005091	2.1631e-04	0.004812	23114.94	8312.07	0.0101
29.48	24.48	0.005134	1.3641e-04	0.005130	36653.77	7797.25	0.0101
24.48	19.48	0.005103	1.6425e-04	0.005267	30442.03	7594.94	0.0100
19.48	14.48	0.005090	1.6217e-04	0.005325	30831.21	7511.46	0.0112
14.48	9.48	0.005014	2.3235e-04	0.006858	21519.48	5832.81	0.0138

Table A.5: UDDS Disharge Test $T = 40\,°C$

SOC_{Start}	SOC_{End}	R_0 (ohm)	R_1 (ohm)	R_2 (ohm)	C_1 (F)	C_2 (F)	RMSE
99.24	94.23	0.004605	-5.3618e-06	0.002597	-932521.12	15400.29	0.006366
94.23	89.23	0.004551	1.3705e-05	0.002869	364832.15	13941.63	0.004807
89.23	84.23	0.004426	7.4617e-06	0.003260	670092.56	12270.77	0.005251
84.23	79.23	0.004396	1.2102e-05	0.003489	413139.01	11465.67	0.005498
79.23	74.23	0.004480	5.0770e-06	0.003532	984841.47	11324.85	0.005908
74.23	69.23	0.004466	8.1730e-06	0.003096	611772.24	12920.36	0.006856
69.23	64.23	0.004428	1.0418e-05	0.002512	479949.85	15920.83	0.011390
64.23	59.23	0.004464	1.0330e-05	0.002635	484046.14	15178.10	0.006272
59.23	54.23	0.004404	1.3386e-05	0.002924	373517.10	13680.44	0.006380
54.23	49.23	0.004410	1.3175e-05	0.003175	379501.65	12599.95	0.006720
49.23	44.23	0.004388	2.2451e-05	0.003417	222704.09	11705.95	0.007173
44.23	39.23	0.004453	3.2434e-05	0.003569	154158.39	11208.92	0.007582
39.23	34.23	0.004399	3.7954e-05	0.003567	131739.68	11212.42	0.008344
34.23	29.23	0.004392	4.0312e-05	0.003527	124033.66	11341.22	0.008168
29.23	24.23	0.004361	5.3062e-05	0.003736	94230.06	10706.15	0.008119
24.23	19.23	0.004421	2.1337e-05	0.003770	234330.58	10610.98	0.008143
19.23	14.23	0.004399	1.9939e-05	0.003702	250769.15	10803.73	0.008864
14.23	9.23	0.004401	2.9109e-05	0.004790	171767.32	8350.95	0.010363

Table A.6: UDDS Charge Test $T = 10\,°C$

SOC_{Start}	SOC_{End}	R_0 (ohm)	R_1 (ohm)	R_2 (ohm)	C_1 (F)	C_2 (F)	RMSE
1.70	6.71	0.0096	2.8361e-03	0.01646	1762.9	2429.7	0.0188
6.71	11.71	0.0096	2.6509e-03	0.01330	1886.1	3008.1	0.0166
11.71	16.71	0.0097	2.4169e-03	0.01511	2068.8	2647.1	0.0174
16.71	21.71	0.0096	2.4579e-03	0.01451	2034.3	2756.7	0.0164
21.71	26.71	0.0097	2.3711e-03	0.01439	2108.7	2780.6	0.0162
26.71	31.71	0.0096	2.3655e-03	0.01409	2113.7	2838.3	0.0159
31.71	36.71	0.0097	2.2452e-03	0.01465	2226.9	2731.1	0.0146
36.71	41.71	0.0095	2.2354e-03	0.01562	2236.8	2560.1	0.0147
41.71	46.71	0.0095	2.2725e-03	0.01651	2200.2	2422.6	0.0155
46.71	51.71	0.0095	2.1766e-03	0.01743	2297.1	2295.5	0.0165
51.71	56.71	0.0095	2.1918e-03	0.01819	2281.2	2199.2	0.0172
56.71	61.71	0.0095	2.1766e-03	0.01887	2297.2	2119.4	0.0177
61.71	66.71	0.0094	2.1037e-03	0.01913	2376.7	2090.6	0.0174
66.71	71.71	0.0094	2.0892e-03	0.01792	2393.3	2232.7	0.0155
71.71	76.71	0.0093	1.9566e-03	0.01882	2555.4	2125.3	0.0154
76.71	78.58	0.0091	2.3156e-03	0.01791	2159.3	2232.9	0.0155
78.58	80.03	0.0090	2.3874e-03	0.01901	2094.4	2104.5	0.0165

Table A.7: UDDS Charge Test $T = 22\,°C$

SOC_{Start}	SOC_{End}	R_0 (ohm)	R_1 (ohm)	R_2 (ohm)	C_1 (F)	C_2 (F)	RMSE
0.92	5.93	0.0079	3.1825e-04	0.00879	15710.8	4550.6	0.0098
5.93	10.93	0.0079	2.3753e-04	0.00713	21049.8	5613.7	0.0093
10.93	15.93	0.0079	1.8929e-04	0.00853	26413.8	4687.0	0.0088
15.93	20.93	0.0079	1.2248e-04	0.00830	40821.4	4821.3	0.0083
20.93	25.93	0.0079	1.9116e-04	0.00824	26156.1	4854.3	0.0086
25.93	30.93	0.0079	1.8585e-04	0.00805	26902.9	4971.2	0.0091
30.93	35.93	0.0079	1.8480e-04	0.00827	27055.9	4834.5	0.0090
35.93	40.93	0.0079	1.2411e-04	0.00891	40286.4	4489.3	0.0089
40.93	45.93	0.0079	1.2633e-04	0.00956	39579.6	4185.2	0.0090
45.93	50.93	0.0080	1.0536e-04	0.01032	47456.8	3877.2	0.0093
50.93	55.93	0.0079	1.2119e-04	0.01107	41256.8	3614.8	0.0099
55.93	60.93	0.0079	1.1468e-04	0.01170	43598.2	3417.8	0.0099
60.93	65.93	0.0079	1.0542e-04	0.01192	47431.4	3355.1	0.0092
65.93	70.93	0.0079	7.6567e-05	0.01066	65301.9	3751.3	0.0080
70.93	75.93	0.0078	7.8356e-05	0.01047	63811.2	3820.9	0.0096
75.93	80.93	0.0077	1.0298e-04	0.01156	48553.0	3460.0	0.0096
80.93	85.93	0.0077	1.1199e-04	0.01297	44647.2	3084.7	0.0104
85.93	90.93	0.0075	8.0737e-05	0.01514	61929.7	2642.2	0.0114
90.93	95.93	0.0072	1.2222e-04	0.01916	40909.1	2087.2	0.0156

Table A.8: UDDS Charge Test $T = 30\,°C$

SOC_{Start}	SOC_{End}	R_0 (ohm)	R_1 (ohm)	R_2 (ohm)	C_1 (F)	C_2 (F)	RMSE
1.19	6.20	0.0070	3.2959e-06	0.00579	1517043	6904.4	0.0085
6.20	11.20	0.0069	7.2621e-06	0.00501	688506	7979.8	0.0078
11.20	16.20	0.0070	1.7673e-07	0.00591	28291853	6772.0	0.0071
16.20	21.20	0.0070	7.2103e-06	0.00563	693456	7102.6	0.0073
21.20	26.20	0.0071	5.4142e-06	0.00562	923492	7119.3	0.0076
26.20	31.20	0.0071	4.7369e-06	0.00558	1055535	7173.4	0.0082
31.20	36.20	0.0070	6.8214e-06	0.00599	732983	6677.0	0.0084
36.20	41.20	0.0070	1.0639e-05	0.00653	469957	6125.3	0.0085
41.20	46.20	0.0070	1.1618e-05	0.00696	430361	5743.8	0.0084
46.20	51.20	0.0071	1.4194e-07	0.00748	35227255	5351.1	0.0081
51.20	56.20	0.0071	5.8525e-06	0.00809	854332	4944.8	0.0077
56.20	61.20	0.0070	1.6291e-06	0.00874	3069128	4578.5	0.0074
61.20	66.20	0.0070	5.7213e-06	0.00903	873930	4430.5	0.0068
66.20	71.20	0.0070	1.9802e-06	0.00779	2524986	5134.4	0.0071
71.20	76.20	0.0070	-1.4306e-06	0.00760	-3495016	5262.0	0.0088
76.20	81.20	0.0068	5.8033e-06	0.00869	861583	4603.0	0.0086
81.20	86.20	0.0068	6.4099e-06	0.00993	780046	4027.3	0.0089
86.20	91.20	0.0067	1.5228e-06	0.01173	3283394	3409.1	0.0090
91.20	96.20	0.0064	7.4638e-06	0.01501	669898	2664.7	0.0110

Table A.9: UDDS Charge Test $T = 40\,°C$

SOC_{Start}	SOC_{End}	R_0 (ohm)	R_1 (ohm)	R_2 (ohm)	C_1 (F)	C_2 (F)	RMSE
1.86	6.87	0.0061	9.8520e-06	0.00259	507512.6	15438.4	0.0177
6.87	11.87	0.0062	3.8105e-06	0.00322	1312156.9	12427.9	0.0069
11.87	16.87	0.0061	1.6378e-06	0.00351	3052926.7	11401.8	0.0070
16.87	21.87	0.0062	3.8219e-06	0.00302	1308259.7	13252.5	0.0073
21.87	26.87	0.0062	4.4317e-06	0.00320	1128231.9	12506.8	0.0072
26.87	31.87	0.0063	4.2561e-06	0.00330	1174773.5	12121.0	0.0084
31.87	36.87	0.0063	3.6945e-06	0.00390	1353360.1	10252.8	0.0078
36.87	41.87	0.0063	1.1127e-06	0.00446	4493583.2	8970.6	0.0086
41.87	46.87	0.0063	-3.0174e-08	0.00473	4183582.1	8464.1	0.0083
46.87	51.87	0.0063	1.2708e-06	0.00507	3934474.0	7891.8	0.0080
51.87	56.87	0.0063	2.8211e-06	0.00544	1772335.3	7347.6	0.0074
56.87	61.87	0.0063	4.2296e-07	0.00572	11821515.1	6988.9	0.0066
61.87	66.87	0.0063	2.8839e-06	0.00589	1733767.6	6789.3	0.0057
66.87	71.87	0.0063	-4.4594e-06	0.00475	-1121231.4	8426.2	0.0089
71.87	76.87	0.0064	-8.5304e-06	0.00467	-586139.1	8560.4	0.0095
76.87	81.87	0.0062	-2.9687e-06	0.00545	-1684224.4	7334.2	0.0091
81.87	86.87	0.0061	2.9529e-06	0.00648	1693247.4	6172.2	0.0089
86.87	91.87	0.0061	2.6429e-06	0.00778	1891852.5	5143.0	0.0084
91.87	96.87	0.0058	4.2784e-06	0.01043	1168673.6	3833.9	0.0071

DEPARTMENT OF SOME SUBJECT OR TECHNOLOGY
CHALMERS UNIVERSITY OF TECHNOLOGY
Gothenburg, Sweden
www.chalmers.se

CHALMERS
UNIVERSITY OF TECHNOLOGY